Review of induced seismicity in geothermal systems worldwide and implications for geothermal systems in the Netherlands

Loes Buijze[1,2] , Lonneke van Bijsterveldt[1], Holger Cremer[3], Bob Paap[1] ,
Hans Veldkamp[1], Brecht B.T. Wassing[1] , Jan-Diederik van Wees[1,2] ,
Guido C.N. van Yperen[3], Jan H. ter Heege[1] and Bastiaan Jaarsma[3]

[1]TNO – Geological Survey of the Netherlands, Princetonlaan 6, 3584 CB Utrecht, the Netherlands; [2]Department of Geosciences, Utrecht University, Princetonlaan 4, 3584 CB Utrecht, the Netherlands and [3]EBN B.V., Daalsesingel 1, 3511 SV Utrecht, the Netherlands

Abstract

Geothermal energy is a viable alternative to gas for the heating of buildings, industrial areas and greenhouses, and can thus play an important role in making the transition to sustainable energy in the Netherlands. Heat is currently produced from the Dutch subsurface through circulation of water between two wells in deep (1.5–3 km) geothermal formations with temperature of up to ~100 °C. As the number of these so-called doublets is expected to increase significantly over the next decades, and targeted depths and temperatures increase, it is important to assess potential show-stoppers related to geothermal operations. One of these potential hazards is the possibility of the occurrence of felt seismic events, which could potentially damage infrastructure and housing, and affect public support. Such events have been observed in several geothermal systems in other countries. Here we review the occurrence (or the lack) of felt seismic events in geothermal systems worldwide and identify key factors influencing the occurrence and magnitude of these events. Based on this review, we project the findings for seismicity in geothermal systems to typical geothermal formations and future geothermal developments in the Netherlands. The case study review shows that doublets that circulate fluids through relatively shallow, porous, sedimentary aquifers far from the crystalline basement are unlikely to generate felt seismic events. On the other hand, stimulations or circulations in or near competent, fractured, basement rocks and production and reinjection operations in high-temperature geothermal fields are more prone to induce felt events, occasionally with magnitudes of $M > 5.0$. Many of these operations are situated in tectonically active areas, and stress and temperature changes may be large. The presence of large, optimally oriented and critically stressed faults increases the potential for induced seismicity. The insights from the case study review suggest that the potential for the occurrence of $M > 2.0$ seismicity for geothermal operations in several of the sandstone target formations in the Netherlands is low, especially if faults can be avoided. The potential for induced seismicity may be moderate for operations in faulted carbonate rocks. Induced seismicity always remains a complex and site-specific process with large unknowns, and can never be excluded entirely. However, assessing the potential for inducing felt seismic events can be improved by considering the relevant (site-specific) geological and operational key factors discussed in this article.

Introduction

The use of geothermal energy is on the rise, as technology improves and the need for CO_2 emission reductions and sustainable energy sources becomes more urgent every day. Geothermal energy can be used for the generation of electricity, and also for heat needed for various industrial processes and heating of, e.g., buildings. Worldwide, the installed geothermal electric capacity increased from 7000 MWe in 1995 to over 20,000 MWe in 2015, and for direct use (heating) the installed capacity increased from 10,000 MWt in 1995 to 70,000 MWt in 2015 (Lund et al., 2015). In the Netherlands the first successful (deep, >1 km) geothermal well was drilled in 2006 at the Bleiswijk Geothermie site. The number of operational doublets increased from 14 in 2017 to 18 in 2019 (excluding the Californië doublets and Heerlen Mijnwater) with a total installed capacity of 194 MWt (Fig. 1A; Table S1 in the Supplementary Material available online at https://doi.org/10.1017/njg.2019.6). Also over 40 exploration licences have been granted (Ministry of Economic Affairs and Climate Policy, 2018). The doublets mostly target porous formations at depths between 2 and 2.7 km with fluid temperatures of 60–100 °C, using this hot water for heating of greenhouses. The current contribution of geothermal energy to the total heat production in the Netherlands is small (0.5%), but is expected to increase significantly (>20%) over the coming decades (Stichting Platform Geothermie et al., 2018). These ambitions
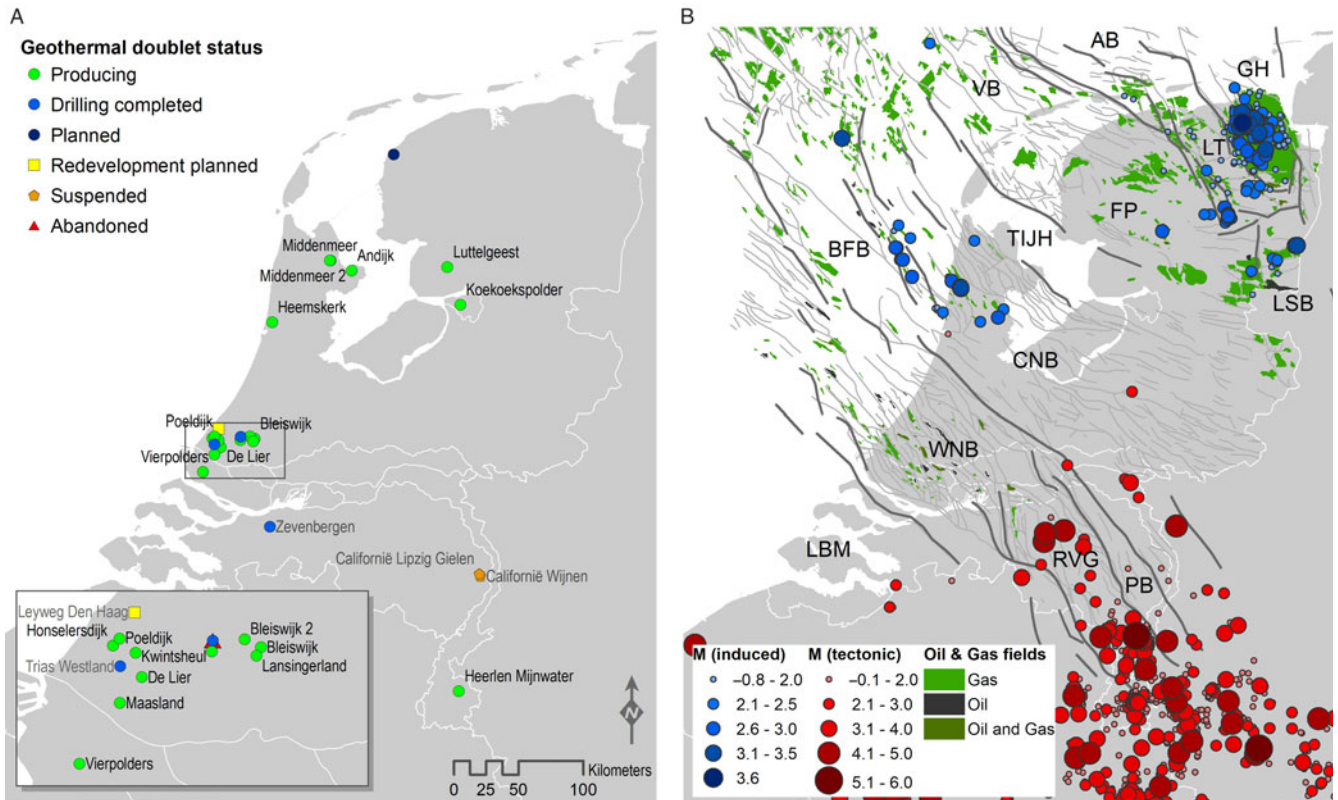
Fig. 1. Overview of geothermal doublets, oil and gas fields, and seismicity in the Netherlands. (A) Geothermal doublets in the Netherlands and their current status (per 1 June 2019). See Table S1 (in the Supplementary Material available online at https://doi.org/10.1017/njg.2019.6) for more information on the doublets. (B) Main structural elements in the subsurface of the Netherlands and boundary fault (thick lines). The thin lines indicate faults in the Permian formations (www.nlog.nl). Oil and gas fields are shown (www.nlog.nl) as well as natural seismicity (red) and induced seismicity (blue) (source: www.knmi.nl, 6 August 2019). AB: Ameland Block; BFB: Broad Fourteens Basin; CNB: Central Netherlands Basin; FP: Friesland Platform; GH: Groningen High; LBM: London–Brabant Massif; LSB: Lower Saxony Basin; LT: Lauwerszee Trough; PB: Peel Block; RVG: Ruhr Valley Graben; TIJH: Texel–IJsselmeer High; VB: Vlieland Basin; WNB: West Netherlands Basin.

require the number of doublets to increase to tens to hundreds. As the Netherlands is now on the brink of a significant increase in geothermal projects, it is important to assess potential hazards associated with these projects. One of these potential hazards is the occurrence of felt and/or damaging induced seismic events (earthquakes).

Induced seismic events have been observed in a number of geothermal projects in other countries, although many systems have been operational for decennia without any seismicity. The occurrence of induced seismicity is not necessarily a problem. The majority of seismic events are not large enough to be felt at the surface in the first place. Also some geothermal projects are situated in remote areas, and/or in areas, such as Iceland, which already have high natural seismicity rates. Here induced earthquakes would go unnoticed and be of no concern, unless event magnitudes become so large that they are felt strongly (Flóvenz et al., 2015). However, in a number of geothermal projects induced seismicity has posed a (serious) problem, causing societal unrest and/or damage to housing and infrastructure. A well-known example was the widely felt event with a local magnitude M_L 3.4 under the Swiss city of Basel caused by development of an Enhanced Geothermal System (EGS), which resulted in infrastructural damage and termination of the project (Häring et al., 2008; Mignan et al., 2015). More recently, a M_w 5.5 event occurred at an EGS site near the city of Pohang, Korea, causing widespread damage and injuring 135 people (Kim et al., 2018a; Ge et al., 2019). Also smaller, non-damaging events can still cause societal unrest. Recent events of M_L 1.8–2.1 near Munich in Germany were

felt by the population and led to a temporary suspension, followed by production at lower flow rates (LIAG, 2018; Seithel et al., 2019). In general, the public is less accepting of induced seismicity than of natural earthquakes (McComas et al., 2016). For the Netherlands in particular, the occurrence of felt seismicity is undesirable as the country is densely populated and induced seismicity due to gas production has already caused damage to >1000 buildings in the north, in the province of Groningen (Fig. 1B). To proceed with the expansion of geothermal technologies in the Netherlands it is highly important to first understand the hazards and the risks and to investigate mitigating the occurrence of felt events as much as possible.

To understand when, where and why felt seismic events can occur in geothermal projects, observations of induced seismicity (or the lack thereof) in projects in other countries can be analysed. These provide insight into the mechanisms and factors controlling the occurrence and size of induced events and provide an overview on how widespread these events are (e.g. Buijze et al., 2019). In this research we present a literature review on the key mechanisms playing a role in geothermal systems, and the occurrences of seismicity observed in geothermal projects worldwide. We focus on deep (>0.5 km) geothermal systems (i.e. excluding shallow aquifer thermal energy storage and heat exchangers) used for heating or generation of electricity. Additionally, we review cases in similar settings where no seismicity has been observed. We place these findings in the context of the (present and future) geothermal target formations and tectonic and geological setting of the Netherlands.
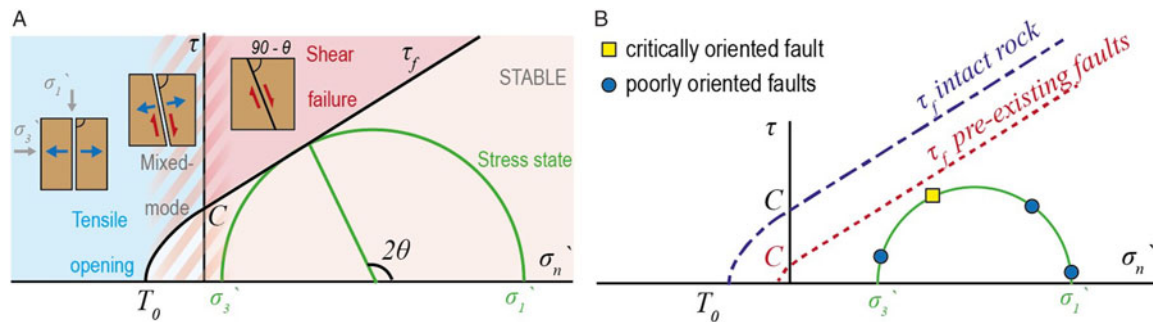
Fig. 2. Mohr diagrams in 2D with failure criteria and example stress state. (A) Mohr diagram with a composite Griffith–Coulomb failure envelope (black line), with tensile strength T_0 and cohesion C. The stress state at shear failure on a fault plane with θ is drawn (green semicircle). Different failure modes (tensile, compressive shear, mixed mode) are illustrated. (B) Mohr diagram with failure lines for intact rocks and pre-existing faults. An example stress state is given (green semicircle) with three different fault orientations relatively far from failure (blue dots) and one fault orientation relatively close to failure (yellow square).

Summary of key mechanisms causing induced seismicity in geothermal fields

Seismicity is the result of rapid slip on a fault plane, which is a pre-existing zone of weakness in the crust. In the upper crust, faulting occurs mainly as a brittle process, which is commonly described by the Mohr–Coulomb criterion (Fig. 2). Sliding can occur when the shear stress τ reaches the failure shear strength τ_f This criterion is defined in terms of the stresses and fault friction:

$$\tau \geq \tau_f = C + \sigma_n' \tan \varphi = C + \sigma_n'\mu \qquad (1)$$

where C is the cohesion, σ_n' is the effective normal stress and φ is the friction angle, the tangent of which is friction coefficient μ (i.e. the slope of the failure line). Normal stress acts as a clamping force, resisting shearing, whereas shear stress promotes shearing. Friction and, in particular, cohesion of intact rocks are higher than for pre-existing faults, which have lower cohesion and may be filled with weak minerals (Fig. 2B).

For induced seismicity, failure on faults is caused by stress changes resulting from anthropogenic activities, such as a gas production or water injection. Note that the initial stress on faults affected by these stress changes is not zero; gravity and plate tectonic loading have imposed an initial stress on the pre-existing faults. The initial fault stress may already be close to failure (critically stressed), depending on the maximum effective principal stress σ_1' and minimum effective principal stress σ_3'. A larger differential stress $\sigma_1' - \sigma_3'$ (large radius of the Mohr circle) and smaller mean effective stress $\sigma_1' + \sigma_3'$ bring the state of stress closer to failure. In addition, the fault orientation in the stress field is important (e.g. the normal of an optimally oriented fault lies in the plane of σ_1' and σ_3' and has an orientation 2θ w.r.t. σ_1'). Reactivation of critically stressed faults may require only small stress changes, whereas reactivation of stable faults requires large stress changes.

Induced vs triggered seismicity

The presence of critically stressed faults is thus of great importance for fault reactivation and the occurrence of induced seismicity. It is also one of the challenges, as very small stress changes can generate relatively large seismic events. In the debate on induced seismicity, such relatively large events have also been called 'triggered' events (not to be confused with events resulting from dynamic triggering by other earthquakes), whereas events requiring a larger stress change have been called 'induced' events. However, it is often

unclear what the stress changes were at hypocentre depth, and how the total energy change of a project is related to the released energy. Moreover, a small stress change can advance the occurrence of an earthquake by hundreds to thousands of years. In this article no distinction is made between triggered and induced; from here all the events linked to a project are termed 'induced'.

Stress changes: pore pressure increase

Pore fluid pressure changes are the most ubiquitous stress perturbation in geothermal systems; pressure changes can occur e.g. due to production and (re)injection of geothermal fluid. An increase in pressure on a fault due to e.g. fluid injection (Fig. 3A) reduces the effective normal stress on the fault and brings the fault closer to failure (Fig. 3D). The elevated pressure diffuses away from the injection well as a function of time, raising pressures and inducing seismic events further away from the source (e.g. Shapiro & Dinske, 2009). Even when injection is terminated, diffusion still causes the pressure to increase at some locations, which may lead to post-injection seismicity. In fact, some of the larger events in Enhanced Geothermal Systems (EGS) have occurred after stimulation was stopped, e.g. at Soultz-sous-Forêts and Basel. When injection occurs in a relatively impermeable but fractured rock mass, the fractures dominate fluid flow and diffusion, whereas for porous rocks the matrix is more important in controlling the fluid flow and diffusion. The pressure distribution thus depends on the rock type targeted and the hydrogeology, as well as on the operational parameters.

Stress changes: poroelastic stressing

A change in pore pressure also causes a volumetric strain (volume change) of the rock mass experiencing a pressure change. This volume change causes a change in stress within the rock mass itself controlled by pore pressure changes, and in the surrounding rock formations, i.e. poroelastic stressing (Fig. 3B). The magnitude of poroelastic stress changes depends on the pressure change, the elastic properties of the rock mass and the geometry of the rock mass experiencing a pressure (e.g. Segall & Fitzgerald, 1998; Soltanzadeh & Hawkes, 2008, 2009). Figure 3B shows an example for a sphere experiencing an increase in pressure. Inside the volume (case 1) the total stresses become more compressive due to the presence of surrounding rock where the hydraulic pressure is still undisturbed. However, due to the increase in pressure the effective stresses become smaller, and the net effect is a more critical stress state (Fig. 3E). To the sides of the expanding (case 2)
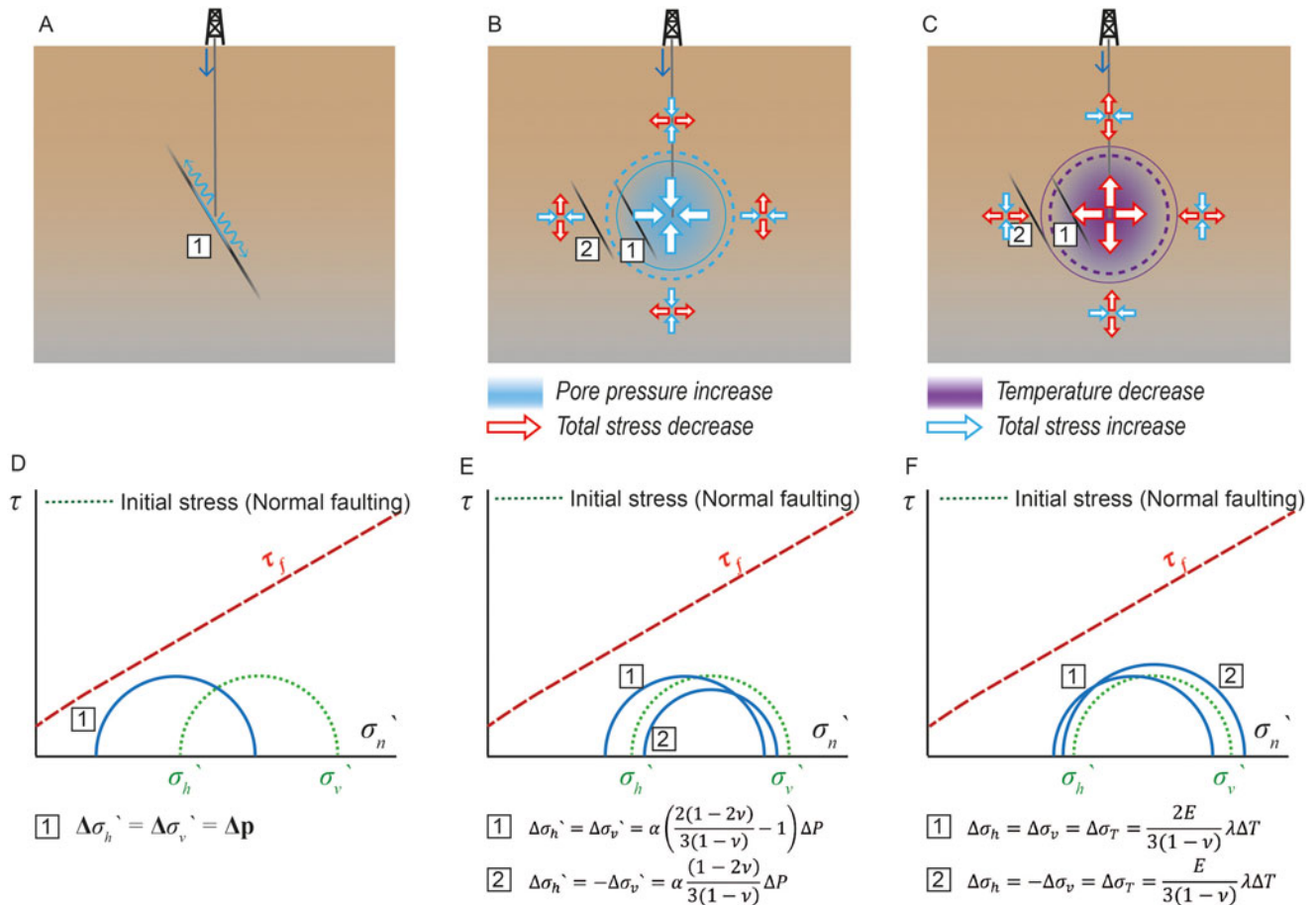
Fig. 3. Simplified examples of the dominant mechanisms causing stress changes in geothermal systems. Examples are given for a normal faulting regime ($\sigma_h < \sigma_H < \sigma_v$). (A) Schematic 2D illustration of pore pressure increases in a fault and diffusion of pressure along the fault. (B) Schematic 2D illustration of poroelastic stressing in and around a spherical pressurised volume. (C) Schematic 2D illustration of poroelastic stressing in and around a spherical cooled volume. Case 1: stresses on a fault within the pressurised or cooled volume. Case 2: stresses on a fault just outside the pressurised or cooled volume. (D–F) Mohr circle diagram showing the stress changes due to scenarios A–C.

volume the horizontal stress becomes more compressive, but the vertical stress decreases, leading to stabilisation in the assumed normal faulting regime. The poroelastic stress-changes outside of the pressurised volume are smaller than inside the volume, and decay rapidly with distance. Poroelastic stressing is expected to play a role both in geothermal systems where pressure is decreased (e.g. producing geothermal fields) or increased (e.g. stimulation in an EGS). Direct pressure effects are expected to dominate near the well, but poroelastic effects reach further at a short timescale. The volume change due to pressure drop can also cause subsidence at the surface, such as observed in many geothermal fields experiencing net extraction, such as the Geysers geothermal field (e.g. Mossop & Segall, 1997) (USA) and Cerro Prieto (Italy) (Glowacka et al., 1999).

Stress changes: thermoelastic stressing

Analogous to poroelasticity, changes in temperature cause volumetric strain of the rock mass, which leads to stress changes within and around the volume experiencing a temperature change. An example for a spherical cooled volume is shown in Figure 3C. The stress changes are opposite to those resulting from a pressure increase, because cooling leads to a decrease in total stresses. In the normal faulting scenario both faults within and just outside the cooled volume become less stable (Fig. 3D). The effect of

temperature changes ΔT may be strong, and is related to pore pressure changes ΔP through (Segall & Fitzgerald, 1998)

$$\frac{\sigma^{\text{thermo}}}{\sigma^{\text{poro}}} = \frac{E\lambda\Delta T}{(1-\upsilon)\alpha\Delta P}$$

where E is Young's modulus, υ is Poisson's ratio and λ is the linear thermal expansion coefficient. Temperature changes and thermoelastic stressing play an important role in geothermal systems. In geothermal fields the temperature difference between the reservoir rock and reinjected water may be in excess of 200 °C, such as at the Geysers and Larderello (Batini et al., 1985; Martínez-Garzón et al., 2014). The difference between the reservoir rock and (re)injected fluids in doublets circulating through hot sedimentary aquifers is smaller but still significant (30–70 °C). Over time (10–30 years) these temperature differences may cause a significant fraction of the rock mass in the doublet system (Willems et al., 2017). The thermal stresses in the vicinity of the wellbore can be significant and lead to tensile failure, but the stresses decrease rapidly with distance (Koh et al., 2011). Note that (for tight rocks) thermoelastic and poroelastic stress changes cannot be simply superimposed as they are coupled processes; e.g. cooling will increase the permeability, which influences the pressure distribution.
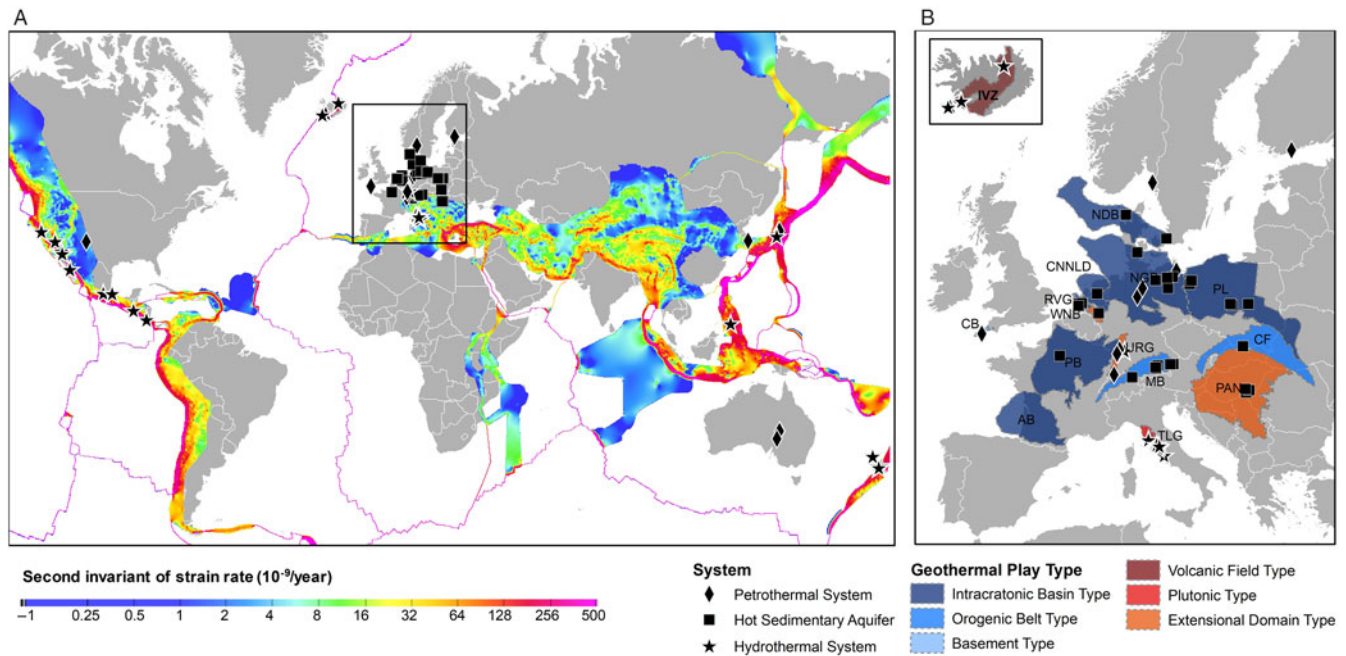
Fig. 4. Map of locations of case studies included in the review. (A) Global map showing location of reviewed cases. Background colours indicate the strain rate magnitude (second invariant of the strain rate tensor) in nanostrains a^{-1}, after the Global Strain Rate Model (Kreemer et al., 2014). (B) Zoomed map of main geothermal regions in Europe and locations of case studies. CB: Cornubian batholith, CF: Carpathian Mountains and Foredeep, IVZ: Iceland Volcanic Zones (combined east, west and neovolcanic zones), MB: Molasse Basin, NGB: North German Basin, NDB: Norwegian–Danish Basin, PAN: Pannonian Basin, PL: Polish Lowlands, RVG: Ruhr Valley Graben, TLG: Tuscany–Latium Geothermal Area, URG: Upper Rhine Graben, WNB: West Netherlands Basin. Shown but not included AB: Aquitaine Basin (modified from Robertson Basins and Plays).

Other mechanisms of fault reactivation

Beside the three main mechanisms discussed above, other mechanisms may also lead to fault reactivation. These include:

- Mass changes: The addition or removal of mass due to the extraction of fluids or mining causes elastic stress changes at depth which may reactivate (critically stressed) faults (e.g. Segall, 1989; Klose, 2007; Kang et al., 2019).
- Excavation-induced stresses: Stress changes around an excavated volume (relevant for mining).
- Chemical changes of fault properties: Rather than changing the stress on fault, changes of the fault properties themselves may bring a fault to failure. These changes result from e.g. the introduction of injection fluids or acid into the subsurface, or temperature changes, which can change the friction coefficient (e.g. Kang et al., 2019). Water can weaken silicate-rich fault rocks through stress corrosion (Davis et al., 1995). Also, dissolution of carbonate can alter the fault properties and cause fault reactivation as proposed for the Molasse Basin (Seithel et al., 2019) or seismicity below impounded reservoirs (Chen & Talwani, 1998).
- Static and dynamic triggering: As one earthquake is induced, stress is redistributed around the fault area that slipped. The stress changes may promote failure on other faults or fault segments (e.g. Schoenball et al., 2012).
- Effects of local geometry: Local heterogeneities may cause the various stress changes to be locally enhanced, e.g. at the interface of layers with strongly different stiffnesses and offset or impermeable faults. For example, subsidence due to large-scale fluid extraction may cause differential strain along faults (Glowacka et al., 1999).

Selection and classification of case histories and definition of key factors

The selection of case histories of induced seismicity linked to geothermal projects was based on the Human Induced Earthquake database HiQuake (Foulger et al., 2018). In this database, 85 geothermal projects related to induced seismicity were listed (http://inducedearthquakes.org, updated December 2018). The cases are situated predominantly in Europe, North America and Asia. Nearly all of the cases listed in HiQuake are included in this study. In addition to these 'seismic' cases, a number of case histories of geothermal projects without induced seismicity were selected for the review. These include cases in the same geothermal regions as the cases with seismicity, and several other regions predominantly in Europe. Closed systems (e.g. heat exchangers), Aquifer Thermal Energy Storage (ATES) projects, and spas were not included. For all cases an additional selection criterion was that the data/information should be publicly available in scientific journals, reports and databases. The cases included in the review are summarised in Table S2 (in the Supplementary Material available online at https://doi.org/10.1017/njg.2019.6), and the locations of cases are shown in Figure 4.

Note that the presence of a local monitoring system may introduce bias towards cases being related to induced seismicity. In the Supplementary Material (available online at https://doi.org/10.1017/njg.2019.6) we include information on the presence of a local monitoring system, and where available the magnitude of completeness M_c is listed. We introduce a cut-off magnitude of M 2.0, above which we classify seismicity as 'felt seismicity', and below which we consider cases 'low-seismic' (following e.g. Evans et al., 2012). A M 2.0 is approximately the threshold for induced events to be felt (e.g. in the Upper Rhine Graben, in the Netherlands), but locally the magnitude from which events can be felt can vary.
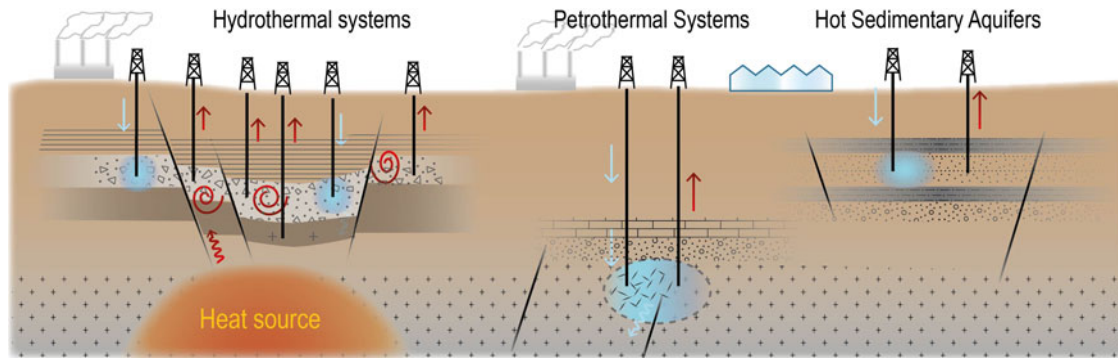
Fig. 5. Schematic illustration of geothermal system types.

Tectonic setting and geothermal play type

The case studies and geothermal regions included in this review are very different in terms of tectonic regime, heat flow, geology, etc. It is useful to classify the cases according to their geothermal play type; here we follow the classification given in Moeck (2014), which is based on the geological controls on the thermal regime, heat flow and hydrogeology. Moeck (2014) distinguishes between conduction-dominated systems and convection-dominated systems, where conduction and convection are indicative of the heat transfer causing the geothermal anomaly. Here we summarise the main characteristics of these systems (Moeck, 2014).

Conduction-dominated systems are found in passive tectonic regions without recent tectonism or volcanism, such as passive continental margins of intracontinental, tectonically quiet areas. Thermal gradients are near-normal, and therefore conduction-dominated systems host mainly low- to medium-temperature geothermal systems. Rock types targeted include mainly sedimentary rocks, and also crystalline basement rocks. In sedimentary basins, heat is transferred mainly through conduction from depth, whereas in crystalline rocks (e.g. granite) heat production is also caused by decay of radioactive elements. Conduction-dominated systems are classified into:

- Intracratonic Basin Type (IBT), which are inactive intracratonic rift basins or passive margin basins (e.g. North German Basin) with a near-normal geothermal gradient. Usually these basins are filled with sediments, which may form permeable aquifers at depths >3 km suitable for the production (and reinjection) of geothermal water. Tighter rock types may require EGS technology (see next subsection).
- Orogenic Belt Type (OBT), which are situated in fold-and-thrust belts and foreland basins (e.g. Molasse Basin). The sediments in the foreland basins are bent and have experienced significant subsidence due to the weight of the nearby mountain belt. Advective heat transport may occur along permeable sedimentary formation from deeper parts to shallower parts further away from the mountain range, causing an elevated geothermal gradient.
- Basement Type (BT), which are related to intrusions or heat-producing element regions (e.g. Cooper Basin). This is an igneous play type consisting of crystalline basement (granite) present below most of the continental area. Natural permeability is often low.

Convection-dominated (CV) systems are high-temperature regions where recent volcanism and/or active plate tectonic processes occur. Examples are magmatic arcs, rift zones, transform fault systems and hot-spot magmatism. Circulation of hot fluids from depth to shallower reservoirs causes an elevated geothermal heat gradient. Convection-dominated systems include:

- Volcanic Field Type (VFT) which are found near magmatic arcs, mid-oceanic ridges, and hot spots (e.g. Icelandic Volcanic Fields, Taupo).
- Plutonic Type (PT) plays, which are related to young orogens and post-orogenic collapse with recent plutonism (e.g. Larderello and the Geysers). Temperatures for both PT and VFT may exceed 300 °C and reservoirs may be vapour- and/or liquid-dominated.
- Extensional Domain Type (EDT) plays, which are situated in metamorphic core complexes, back-arc extension, pull-apart basins and intracontinental rifts (e.g. Upper Rhine Graben, the Great Basin). In contrast to the previous cases, this is a non-magmatic play type, where heat flow predominantly occurs by convection through permeable faults. The crust in these regions is usually thinner, creating a higher geothermal gradient.

Fluid flow and convective heat flow is dominated by matrix porosity (VFT) and/or fractures (EDT, PT).

Figure 4B shows the geothermal play types of the main geothermal areas in Europe. Natural seismicity in the convection-dominated regions is much more ubiquitous than in the conduction-dominated systems, which may make distinguishing natural and induced seismicity difficult (e.g. Brodsky & Lajoie, 2013).

Geothermal system type

Depending on the tectonic setting and rock type, different types of deep geothermal energy systems exploit the geothermal resources. Here three different types are recognised (following Breede et al., 2015): hydrothermal systems (HS), petrothermal systems (PS) and hot sedimentary aquifers (HSA) (Fig. 5).

- Hydrothermal systems (HS), also called geothermal fields, are the oldest geothermal systems and are situated in tectonically active, convection-dominated settings (see Fig. 4A). These fields are high-temperature (>200 °C) reservoirs at shallow depth (<~3 km) and can be classified as vapour-dominated or water-dominated fields. Permeability of the matrix and/or fractures is high enough to allow flow without stimulation. Well-known examples include the Geysers, and Larderello. From the early 1900s, hot water from these fields was used for heating (direct-use) and the first commercial production of electricity

was achieved in 1926 at Larderello. The fields can be extensive (>10 km) and contain numerous wells. Initially the fields only produced steam and/or hot water. From the 1970s, reinjection of produced cooled water as a means of disposal and/or pressure maintenance became common practice (Stefansson, 1997; Kaya et al., 2011). Note that reinjection may not necessarily occur in the producing formation but could also occur shallower or in a different area of the field.

- Petrothermal systems (PS) (here also called EGS) target rocks that have a low permeability and need to be stimulated before fluid flow can be achieved. These include the Hot-Dry Rock (HDR) concept, where wells are connected through hydraulic fracturing which is achieved by injection pressures exceeding the minimum principal stress (e.g. Jung, 2013) and Enhanced Geothermal Systems where injection at high pressures (but lower than the minimum principal stress) stimulates the permeability of the natural fracture network between two wells by shearing. Since the 1980s a number of pilot-EGS projects have been conducted, and the first commercial plants are operational (Lu, 2018). In this review both initial HDR project and EGS projects are classified as PS. Typically a petrothermal system is exploited by circulation between two wells. Note that there may also be EGSs within geothermal fields, e.g. in the Geysers (PS–HS).
- Hot sedimentary aquifers are porous/permeable sedimentary rock formations where heat flow is dominated by conduction (see Fig. 4A). Mostly these are low–moderate-temperature (30–150 °C) systems in permeable sedimentary aquifers at relatively shallow depth (1–4 km). Typically, water is circulated between two wells (a doublet) at low pressures. Temperatures can be high enough for electricity generation (e.g. in some systems near Munich) but are mostly suitable for direct use in e.g. district heating, space heating and various other applications (e.g. North German Basin, Paris Basin, the Netherlands).

Beside the type of geothermal system, also the depth and reservoir temperature are specified for the case histories included in the review. In addition, the minimum vertical distance of the geothermal system to basement was listed. For HSA and PS this was usually the crystalline basement. For hydrothermal systems where no crystalline basement was present, this could be another rock type, e.g. greywacke (Taupo Volcanic Zone in New Zealand).

Geological parameters

The initial stress is very important for assessing the reactivation potential of faults. However, *in situ* stress measurements are often not available, and often faults have not been identified. Where available the stress regime was listed, with NF: normal faulting, NF-SS: transtensional faulting, SS: strike-slip faulting, SS-TF: transpressive faulting, and TF: thrust faulting. For each activity the rock type of the geothermal target formation is listed, as rock type may influence the potential for faulting and controls fluid flow. Also an indication of the average matrix porosity Φ was included. Where no porosity data were available, a standard value of 1% was assumed for granites, 8% for carbonates and 10% for volcaniclastic sequences. To analyse whether there is a relation between tectonic activity and induced seismicity, at each locality the second invariant of the strain tensor (i.e. strain magnitude) was obtained from the Global Strain Rate Model v2 (Kreemer et al., 2014) (Fig. 4A).

Operational parameters

Operational parameters are also important for the occurrence of induced seismicity, as larger pressure and temperature changes result in larger stress changes. For each activity we list the start of operations, and the following operational parameters:

- ΔV (m³): net injected volume
- ΔP (MPa): maximum injection pressure at the wellhead
- ΔT (°C): temperature difference between reservoir temperature and (re)injected fluids

Seismicity

If seismic events occurred, the maximum magnitude and the date of occurrence are listed, as well as the magnitude scale that was used. In addition, where available the magnitude of completeness M_c of the local monitoring network was listed.

Seismicity in geothermal systems: case history review

Here we summarise the main findings from the case history review. We start with a brief summary of the characteristics of the main geothermal regions in which the selected case histories are located; for more extensive reviews of individual cases we refer the reader to e.g. Evans et al. (2012), Foulger et al. (2018) and the references therein. The geothermal plays in the Netherlands are not included here but are described more extensively in the Implications section further below. After summarising the different geothermal regions and observed seismicity, we discuss the dominant geological and operational factors underlying the occurrence of induced seismicity in different geothermal systems.

Conduction-dominated plays and case studies

North German Basin: The North German Basin (Fig. 4B) is a Permian rift basin (IBT) with a thick infill of Mesozoic and Cenozoic sediments (e.g. Scheck-Wenderoth & Lamarche, 2005). It is a sub-basin of the Central European Basin System. The basin is inactive, and natural seismicity rates are low. The main geothermal target formations are sandstone aquifers from the Lower Jurassic Lias, the Upper Triassic Keuper (which includes the well-known Rhaetian Formation) and the Lower Triassic Bundsandstein sandstones including the Dethlingen, Volpriehausen sandstones (Franz et al., 2018). Starting in 1986 at Waren, five doublets (Neustadt-Glewe, Neubrandenburg, Neuruppin, Sønderborg and Waren) circulate water through the low-temperature (45–100 °C), porous (20–30%) Liassic and Keuper sandstone aquifers at depths of 1–2.5 km (Kabus & Jäntsch, 1995; Seibt et al., 2005; Røgen et al, 2015; Franz et al., 2018). Apart from an incidental acid stimulation, no stimulation techniques are required and high flow rates can be attained at low injection pressures (<1 MPa). The deeper, tighter Bundsandstein (4.1 km, 150–170 °C) in the west was hydraulically fractured in two geothermal research projects: Genesys Hannover and Horstberg (Orzol et al., 2005; Rioseco et al., 2013; Tischner et al., 2013). Similarly, the geothermal potential of older Permian Rotliegend sediments and volcanics was tested by hydraulic fracturing at the Gross Schönebeck research well (e.g. Zimmermann et al., 2010).

Only very small events occurred during the hydraulic fracturing experiments, with maximum magnitudes of M_w-1 at Gross Schönebeck (Moeck et al., 2009; Kwiatek et al., 2010; Blöcher et al., 2018), or no events at all (Tischner et al., 2013). At the other
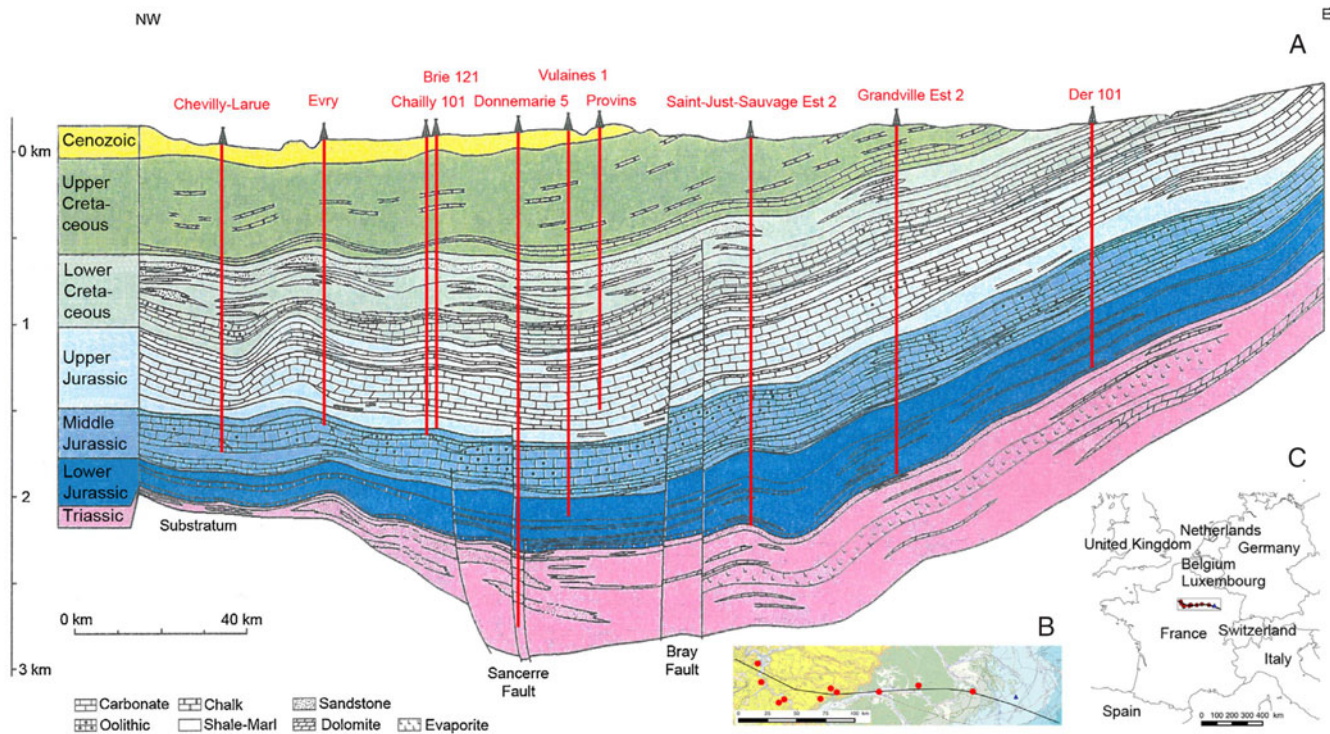
Fig. 6. Cross-section of the stratigraphy of the Paris Basin (Dentzer et al., 2016, reprinted with permission from Elsevier).

sites no monitoring was in place, but no events have been reported by the public.

Norwegian–Danish Basin: The Norwegian–Danish Basin (Fig. 4B) is a Permian rift basin which is also part of the Central European Basin System (IBT). The thickness of the sedimentary cover ranges from 1–2 km in the south to 9 km in the north of the basin (Frederiksen et al., 2001). The main geothermal targets are the Upper Triassic Gassum (Rhaetian in Germany) and the Lower Triassic Bundsandstein (Kristensen et al., 2016). Two geothermal plants are operative: Thisted (started in 1984) and Margretheholm (started in 2005) near Copenhagen. Thisted exploits the high-porosity (26%) Gassum sandstone at 1.2 km depth with a temperature of 45 °C (Mahler, 1995; Hjuler et al., 2014; Røgen et al., 2015). The Margretheholm plant targets the Bundsandstein at 2.5 km depth (73 °C) (Mahler et al., 2013), which directly overlies the granitic basement (Erlström et al., 2018).

No seismic events have been reported for either geothermal plant.

Paris Basin: The Paris Basin is a Permo-Triassic basin in northern France with a sediment thickness up to 3 km in the centre (Fig. 4B). The absence of microseismicity and absence of horizontal motion indicates the basin is tectonically inactive (Cornet & Röckel, 2012). The prime geothermal target in the Paris Basin is the ~200 m thick Middle Jurassic Dogger carbonates (1.5–2 km, 55–85 °C) (Lopez et al., 2010). The most productive layers in the Dogger strata are permeable oolitic reef deposits and shelf sediments with a net thickness of 15–25 m, with an average porosity of 15%. The fluid flow is generally matrix-controlled, although in some parts fluid flow may locally be fracture-controlled (Rojas et al., 1989). The Dogger is underlain by Lower Jurassic shales, Triassic sands and shales, which are underlain by the granitic basement (Fig. 6). Between 1970 and 1985 more than 100 geothermal wells were drilled in the Paris Basin, mainly used for district

heating. Of the 55 doublets 34 are still operational, without any thermal decline (Lopez et al., 2010). Hydraulic stimulation is not necessary, and circulation can occur at low injection pressures (<1 MPa). However, chemical stimulation is sometimes used to improve the injectivity (Ungemach et al., 2005).

No (felt) induced events have been reported for any of the doublets in the Paris Basin. No site-specific monitoring is in place.

Polish Lowlands: The Polish Lowlands, or Polish Basin, is another sub-basin of the Central European Basin System, which formed during rifting in the Permian (e.g. Scheck-Wenderoth & Lamarche, 2005). The basin was filled with >8 km of Mesozoic sediments, with the Polish trough as the deepest part of the basin running NW–SE (e.g. Grad & Polkowski, 2016). The main aquifers targeted by geothermal operations in the Polish Lowlands are the porous Lower Jurassic (0.7–3.7 km depth, 25–120 °C) and Lower Cretaceous (0.8–2.8 km depth, 30–85 °C) sandstone formations which have porosities of 5–20% with an average permeability for the Lower Jurassic of 1.1×10^{-12} m^2 (Kurowska, 2000; Sowizdzal, 2018). Since 1996 five geothermal plants have become operational that use hot water from these aquifers for district heating (Pyrzyce, Mszczonów, Uniejów, Stargard Szczecinski and Poddebice), as well as several spas (e.g. Meyer and Kozlowski, 1995; Górecki et al., 2015; Kepinska, 2015). The systems at Poddebice and Mszczonów (Bujakowski & Wojnarowski, 2005) only produce the formation water, whereas the others circulate fluids between the wells.

No (felt) induced events have been reported for any of the system in the Polish Basin. No local monitoring stations are present.

Molasse Basin: The Molasse Basin is a foreland basin north of the Alps (OBT), stretching from Switzerland in the west through the south of Germany to Austria in the east (e.g. Reinecker et al., 2010). The geothermal target formation is the permeable, faulted, karstified Upper Jurassic Malm limestones which underlie the
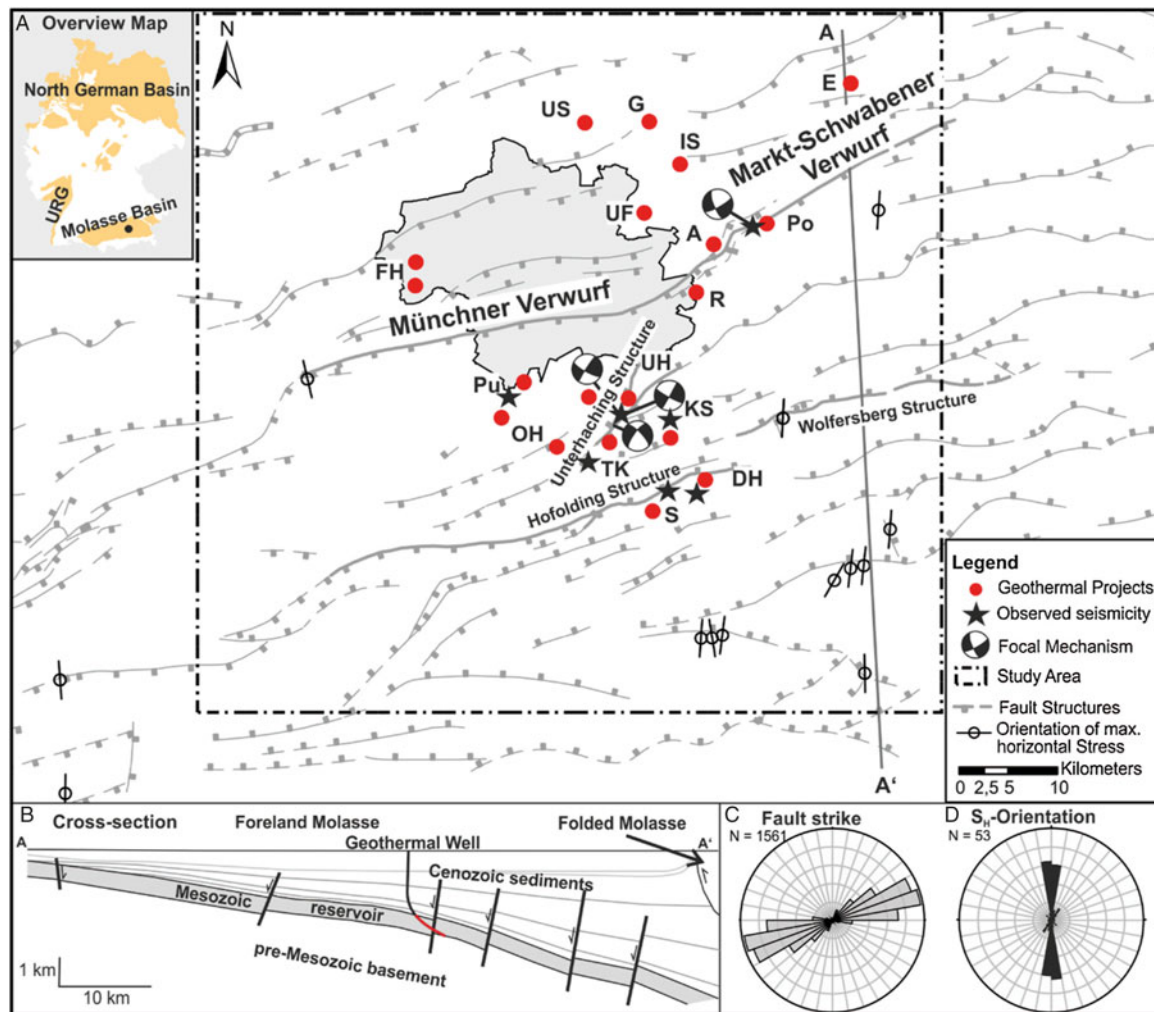
Fig. 7. Overview of geothermal systems in the Munich area in the Molasse Basin. (A) Overview map showing Munich, the location of geothermal projects, and local fault structures. (B) Cross-section of the Mollasse Basin (Seithel et al., 2019, reprinted with permission from Elsevier).

Tertiary Molasse sediments. Near Munich the Malm lies at a depth of 3 km, with a thickness of over 600 m, with temperatures in the range 85–130 °C (e.g. Seithel et al., 2019). Here, the Malm directly overlies the Variscan basement (Fig. 7). Further to the west at Sankt Gallen in Switzerland, Middle Jurassic and Triassic and Permian sediments are found below the Malm (Moeck et al., 2015). So far, a total of 26 geothermal doublets are operational in the Molasse Basin, 16 of which are situated around Munich (Agemar et al., 2014; Baumann et al., 2017; Seithel et al., 2019), and 7 of which are located in the east of the basin near the German–Austrian border (e.g. Goldbrunner, 1999; Karytsas et al., 2009). The geothermal wells often target faults because of the enhanced permeability. Most of the doublets are used for district heating, and three systems (Dürrnhaar, Kirchstockach and Sauerlach) to the south of Munich generate electricity (Wanner et al., 2017; Seithel et al., 2019). Circulation occurs at low (1–2 MPa) pressure (e.g. Wanner et al., 2017), and hydraulic stimulation is not required.

Three geothermal sites in the Molasse Basin are associated with induced events with $M > 2.0$ (Fig. 7). The most well-known example is Sankt Gallen, where a M_L 3.5 event was recorded during well control operations following influx of gas (Kraft et al., 2013; Obermann et al., 2015; Diehl et al., 2017). Other felt events of M_L 2.4 and M_L 2.1 were recorded during circulation in doublets

at Unterhaching (Megies & Wassermann, 2014) and Poing (LIAG, 2018; Seithel et al., 2019), respectively after a few months and after 5 years of circulation. In both cases the events occurred in the top of the crystalline basement underlying the Malm. A number of other sites were associated with $M < 2.0$ events: Dürrnhaar (M_L 1.3), Sauerlach (M_L 1.2), Kirchstockach (M_L 0.8), Oberhaching (M_L 0.5), Taufkirchen (M_L 0.3), Pullach, M_L 0.4) (Seithel et al., 2019) and other systems around Munich have not shown any seismicity, even though the monitoring system captures all events with $M > 1$ .0–1.5 (and locally even smaller events). Also no events have been reported for the doublets in the eastern part of the basin.

Cooper Basin: The Cooper Basin is located in a stable region of the northeast of Australia. The geothermal target formation is a large naturally fractured granitic body covered by 3.6 km of sediments. Heat is generated within the granite, causing high temperature gradients in the area. Two EGS doublets are present at the Habanero geothermal field (Baisch et al., 2006, 2009), and one EGS well in the Jolokia field (Baisch et al., 2015).

More than 60,000 events (M_L 1.6 to 3.7) were detected during three hydraulic stimulations: two in Habanero 1 and one in Habanero 4 (Baisch et al., 2006, 2009, 2015). Maximum magnitudes were M_L 3.7, M_L 3.0 and M_L 3.0, and the microseismic cloud

revealed a large thrust fault structure that was well-oriented in the regional stress field and was reactivated by the injection (Holl & Barton, 2015). Stimulation of the Jolokia well on the other hand resulted in smaller events ($M_L < 1.6$); here the well did not intersect a large fault (Baisch et al., 2015).

EGS Helsinki: Recently, fractured granitic basement rocks of the Svecofennian province (part of the Fennoscandian shield) were targeted with EGS technology below the city of Helsinki, Finland (Kwiatek et al., 2019). Here, the crystalline basement can be found almost up to the surface. Natural seismicity rates in the south of Finland are low, and in the years prior to the stimulation only small natural earthquakes up to M 1.7 were recorded in the vicinity of the drill site. The stress regime is strike-slip. The well OTN-3 was drilled to 6.1 km deep, where temperatures of 125 °C were measured. The well was stimulated by injecting 18,160 m³ of fresh water, at wellhead pressures of 60–90 MPa, and flow rates of 400–800 L min⁻¹.

Seismicity was recorded during the stimulations ($M_c - 1.2$) and processed near-real-time (Kwiatek et al., 2019). Depending on the evolution of seismic magnitudes in relation to the injected volume, injection flow rates were adjusted. A total of 6150 events were recorded, with a maximum magnitude M_w of 1.9.

Other: Other EGS and HDR test sites targeting granitic basement rocks or tight sandstones included in the database are Fenton Hill (Phillips et al., 1997), Fjällbacka (Jupe et al., 1992), Paralana (Albaric et al., 2014; Riffault et al., 2016) and Rosemanowes (Batchelor, 1982; Richards et al., 1994; Parker, 1999; Evans et al., 2012); see further Table S2 (in the Supplementary Material available online at https://doi.org/10.1017/njg.2019.6). Maximum magnitudes during stimulations at these sites were respectively M 1.3, M_L 0.2, M_L 2.5 and M 2.0. At Fjällbacka, during a later stimulation, an event was felt but its magnitude was unknown.

Convection-dominated plays and/or case studies

Iceland Volcanic Zones: Iceland is the site of active rifting and volcanism (VFT) and has large geothermal potential. The Icelandic volcanic area runs SW–NE across the island and is seismically active. Production of geothermal energy started in the 1970s. Currently eight high-temperature (230–440 °C) fields are being produced (six of them for electricity), and tens to hundreds of low-temperature fields for district heating (Ragnarsson, 2005; Armannsson, 2016). Reinjection occurs in five high-temperature and four low-temperature fields (Flóvenz et al., 2015). The main geothermal reservoir rocks are basaltic lava flows and hyaloclastics, which may have high porosities (e.g. Eggertsson et al., 2018).

The Iceland Volcanic Zones are well covered by the seismic network, with a magnitude of completeness of ~1.0 (Panzera et al., 2017). Seismicity was observed in most of the fields where reinjection occurred, with maximum magnitudes between M_L 2.0 and 4.0 (Flóvenz et al., 2015). The largest event, of M_L 4.0, was observed at the Húsmúli reinjection site in the Hellisheidi field (Juncu et al., 2018).

Taupo Volcanic Zone: The Taupo Volcanic Zone (TVZ) is a 150 km long NE–SW zone in the centre of the North Island, New Zealand. The TPV is a zone of active rifting and volcanism associated with subduction at the Kermadec trench in the east (Wilson & Rowland, 2016). Currently 16 geothermal fields are being developed in the region, mostly targeting pyroclastic, fractured lavas (andesites, rhyolites), and fractured greywacke basement formations at 1–3 km depth (250–320 °C). Porosities vary

from several per cent in the deeper rocks to more than 20% in the shallower rocks (Henrys & Hochstein, 1990; Cant et al., 2018). Production started in the late 1950s from the Kawerau and Wairakei fields, generating electricity and producing warm water for district and industry heating. Reinjection started from the 1980s.

Local monitoring networks are present near most geothermal fields so that most events with $M > 2.0$ are detected (Sherburn et al., 2015a). Induced seismicity was observed in a number of fields, notably Rotokawa (M 3.3), Kawerau (M 3.2), Mokai (M 3.2), Ngatamariki (M 2.7) and Wairakei (M 2.5) (Sherburn et al., 2015a). A clear correlation with reinjection wells could be observed for some of those fields (Sewell et al., 2015; Sherburn et al., 2015b). Several other fields in similar settings (Ohaaki, Ngawha) have not shown seismicity.

The Geysers: The Geysers field in Northern California is the largest producing geothermal field in the world. It lies 80 km from the San Andreas Fault between large active strike-slip faults, in a transtensional stress environment (Garcia et al., 2016). The Geysers field itself is bounded by two NNW–SSE-striking faults that have been inactive for at least 15,000 years, and is underlain by a granitic pluton. The reservoir is vapour-dominated and situated in faulted metagreywacke (tight, competent, metamorphosed, poorly sorted sandstone). The reservoir can be divided into a normal-temperature reservoir (NTR) (~1–2.6 km, $T < 240$ °C), and a high-temperature reservoir (HTR) which underlies the NTR in the northwest Geysers ($T > 400$ °C) (Garcia et al., 2016). Geothermal production started in 1960, and reinjection started in the early 1980s as field pressures decreased (Majer et al., 2017). Currently 60–80% of the water is reinjected. In the northwest of the Geysers an EGS demonstration project is being developed (Rutqvist et al., 2015; Garcia, et al., 2016).

Since the early 1980s, more than 750 events have been recorded annually in the Geysers geothermal field.

Since 2003, 20 $M > 4.0$ events have been recorded, with the maximum, M_w 5.0, occurring on 14 of December 2016 (Majer et al., 2017). The events show a strong spatial correlation to the (re)injection wells (Martínez-Garzón et al., 2014) and a temporal correlation to injected volumes (Trugman et al., 2016).

Tuscany–Latium: The Tuscany–Latium geothermal region is situated in the west of Italy. The high heat flow derives from the post-orogenic collapse of the Apennines, which causes extension and magmatism (Batini et al., 2003). Recent seismic activity is moderate (M 4.1 in 1970), but in 1724 a large event occurred in the region, with intensity up to VII–VIII (Batini et al., 1985). The northern geothermal fields (Larderello-Travale, Monte Amiata) are characterised by a shallow reservoir (<1 km, T up to 250 °C) composed of evaporitic rocks and limestones, and a deeper reservoir (2.5–3.5 km, $T > 350$ °C) composed of fractured metamorphic rocks (Giovanni et al., 2005). The southern fields (Torre Alfina, Latera, Cesano) target fractured limestones at 0.6–2.0 km depth ($T < 230$ °C) (Cavarretta et al., 1985; Buonasorte et al., 1995; Evans et al., 2012). Larderello-Travale is the oldest steam-producing geothermal field, with the first commercial powerplant in 1926.

Seismicity in the fields clustered around (re)injection wells and reached moderate magnitudes up to M_L 3.2 at the Larderello–Travale field (Batini et al., 1985). A M_w 4.5 (M_L 3.9) occurred in April 2000 near the Piancastagnaio field at Monte Amiata (Mazzoldi et al., 2015; Braun et al., 2018), but the relationship with geothermal operations was difficult to identify due to high natural seismicity in the region and poor available seismic data.

Several injection tests were performed, but not all tests resulted in significant seismicity. At Latera several injection tests only induced magnitudes up to 0.8 (Moia, 2008).

Salton Sea: The Salton Sea geothermal field (Southern California) is located at the transition from the diverging East Pacific Rise to the strike-slip San Andreas Fault system (McGuire et al., 2015). The field is situated in a seismically active transtensional region between strike-slip faults. It is a water-dominated geothermal field located in sandstone, siltstone and shale, which are slightly altered at shallow levels (1–2 km and <280 °C) and more altered and cemented at deeper levels where temperatures exceeded 300 °C. Porosity in the shallow formations is 10–30% but decreases strongly with depth and alteration. Deeper rocks are, however, extensively fractured, which provides permeability. Production of steam started in 1986, and was increased to 5–10 million m³ per month from the 1990s, of which 80% was reinjected. With increasing scale of operations the seismicity rates increased. From 1985 to 2011 over 12,000 earthquakes with $M > 1.7$ were recorded, mostly between 3 and 7 km depth (Brodsky & Lajoie, 2013). The largest observed event was a M 5.1. which was part of a large earthquake swarm with multiple $M > 4$ events. However, the correlation with operational parameters was less straightforward than e.g. at the Geysers; an initial correlation with production rates was observed, but also tectonically driven earthquake swarms occur in and near the field (Brodsky et al., 2013; Trugman et al., 2016).

Great Basin: The Great Basin is a large basin in the west of the USA, characterised by active dextral strike-slip faulting and extensions, i.e. a transtensional stress regime. Geothermal systems in the basin are found near active zones of intersecting or overlapping faults, such as step-over fault systems, which provide permeable pathways for hot fluids, but rarely near mature fault zones, as these may have lower permeability (Faulds et al., 2010). The main geothermal target formations are metavolcanics and metamorphic (siliceous metamudstone) rocks at 150–250 °C (e.g. Lutz et al., 2010). In a few cases at the western margin, heat flow is of magmatic origin (e.g. at Coso field, $T = 285$ °C). Here the main reservoir rock is (grano)diorite (Davatzes & Hickman, 2010). Over 400 geothermal systems are found in the Great Basin, 27 of which have temperatures high enough for generation of electricity.

For most systems no induced seismicity is reported, but local monitoring systems were only placed near a couple of geothermal fields. Several small events were measured during EGS stimulation at Desert Peak with M_L up to 1.7 (Benato et al., 2016) and production and reinjection in Brady's field with M_L up to 2.4 (Cardiff et al., 2018). At Brady, no seismic events were observed when pumping rates were high, but events were temporally correlated to times when production was halted. Larger magnitudes ($M < 4.4$) occurred in the high-temperature field Coso in the western margin of the basin (Trugman et al., 2016).

Pannonian Basin: The Pannonian Basin (Fig. 4B) is a back-arc basin that started to form in the early Miocene through rifting and volcanism, and covers Hungary as well as parts of Croatia, Slovakia, Slovenia and Romania (Horváth et al., 2015). Present-day inversion causes transpressive stresses, and seismicity occurs in the basin with magnitudes up to M 6.0 (Tóth et al., 2008). The prime geothermal target is the 100–300 m thick base of permeable (10^{-13}–10^{-12} m²) Ujfalu Formation (1–2 km, 30–100 °C), which consists of high-porosity (20–30%) unconsolidated sediments (sands) overlying an aquitard formation (Horváth et al., 2015). A second target is karstified Mesozoic carbonates at depths <2 km. There are over 350 sites producing thermal water mostly

from the Ujfalu Formation, of which >150 are used for space heating. Most geothermal systems such as for example Szentes (Szanyi & Kovács, 2010; Bálint & Szanyi, 2015) consist of multiple wells, and only produce water, which over time leads to pressure decreases in the geothermal aquifer. Reinjection occurs in only 20 wells, for example in the Hódmezővásárhely geothermal system (Szanyi and Kovács, 2010) and in the Orosháza-Gyopárosfürdő geothermal system (Szita and Vitai, 2013).

No seismicity has been reported for any of the geothermal sites. No local networks are in place; the regional network has a detection threshold of ~M 2.0 (Tóth et al., 2008).

Pohang: The Pohang EGS site is located in the Pohang Basin in the southeast of the Korean Peninsula and targets a granodioritic intrusion found from 2.4 km depth (Kim et al., 2018a). The Pohang Basin is a Miocene back-arc basin which is currently subject to a compressive stress regime, and although natural seismicity in the vicinity of the EGS is low, earthquakes with M_w 5.8 have occurred at 40 km from the EGS site (Kim et al., 2018b). Two wells (PX-1 and PX-2) were drilled to a depth of 4.2 km with a horizontal distance of 0.6 km between them. The temperature at this depth was 140 °C.

Between 29 January 2016 and 18 September 2017 five hydraulic stimulations were performed, three of them in PX-2 (the first, third and fifth) and two of them in PX-1 (the second and fourth) (Kim et al., 2018a). The maximum wellhead pressures were reached during the first two stimulations and were 89.2 MPa (PX-2) and 27.7 MPa (PX-1) (Ge et al., 2019). A total volume of 7135 m³ was injected into PX-2 and 5663 m³ into PX-1, of which 2989 m³ and 3968 m³ was flowed back, so that the net injected volume in both wells was ~6000 m³. Injection tests indicated that a hydraulic barrier was present between PX-1 and PX-2.

During drilling of PX-2 a fault zone was encountered at 3.8 km depth. This resulted in mud losses, and seismicity of up to M_w 0.9 (Ge et al., 2019). Seismicity with magnitudes up to an M_w 3.2 in April 2017 was recorded during the various stimulations in PX-1 and PX-2. Injection in PX-2 had reactivated the fault zone which penetrated by the well at 3.8 km depth. The third and last stimulations of PX-2 in September 2017 produced only small-magnitude seismicity up to M_w 2.0 on this fault. However, seismicity restarted in mid-November 2017, with some foreshocks increasing in magnitude from M_w 1.6 to M_w 2.7. Subsequently, on 15 November 2017 the M_w 5.5 mainshock occurred at 4.3 km depth, just below the location of the foreshocks and seismicity previously induced by injection in PX-2 (Grigoli et al., 2018; Kim et al., 2018a; Ge et al., 2019). A first-order hydromechanical modelling approach suggests that the pressure increase at the hypocentre depth was only 0.07 MPa, indicating the fault was close to failure (Ge et al., 2019).

Upper Rhine Graben: The Upper Rhine Graben is a 300 km long NNE–SSW-trending active rift system on the border of France and Germany. The graben is seismically active, with frequent small events and occasional moderate-sized events, and some historic events of M ~7.0 (Grimmer et al., 2017). Five medium- to high-temperature geothermal power plants are currently operational in the graben (Vidal & Genter, 2018). The wells at Basel (terminated) and Soultz-sous-Forêts target the fractured granitic basement at 3.5–5 km depth with temperatures of 160–200 °C (e.g. Cornet et al., 1997; Baria et al., 1999; Häring et al., 2008; Dorbath et al., 2009; Deichmann et al., 2014). The geothermal systems at Insheim, Landau and Ritterhofen were developed using a multi-reservoir concept, where the interface of the granitic basement and the overlying tight, fractured sediments are

both targeted (e.g. Schindler et al., 2010; Maurer et al., 2015; Baujard et al., 2017; Küperkoch et al., 2018; Vidal and Genter, 2018). At Bruchsal, only the tight, fractured Triassic–Carboniferous sandstone sediments were targeted at a depth of 2.5–3.5 km at a temperature of 100–150 °C (Meixner et al., 2016). Hydraulic stimulation of the pre-existing fracture network was required except at Bruchsal, and typically volumes between 10,000 and 50,000 m^3 are injected at wellhead pressures between 15 and 30 MPa, except at Rittershofen where pressures were lower (Baujard et al., 2017).

Seismicity was monitored in most geothermal systems. At a number of sites felt events were induced, with the largest event being a M_L 3.4 related to the Basel EGS stimulations (e.g. Häring et al., 2008; Deichmann et al., 2014). At other locations seismicity was smaller, but still felt by the local population, e.g. a maximum M_L 2.9 at Soultz-sous-Forêts after stimulation (e.g. Cornet et al., 1997; Charléty et al., 2007; Dorbath et al., 2009), a M_L 2.7 at Landau during circulation (Bönnemann et al., 2010) and a M_L 2.4 at Insheim (Küperkoch et al., 2018). Events occurred both during stimulation and circulation, and were located predominantly in the granitic basement (Pilger et al., 2017; Küperkoch et al., 2018). However, felt events did not always occur; at Rittershoffen, close to Soultz-sous-Forêts, the maximum magnitude did not exceed M_L 1.6 (Baujard et al., 2017; Lengline et al., 2017). At Bruchsal also no seismicity was recorded during circulation, even though a local monitoring network was present with a magnitude of completeness of M_L 0.7 (Gaucher, 2016).

Japan: Japan is a tectonically active country with active volcanism and has large geothermal potential, with the first commercial geothermal powerplant opening in 1967 at Matsukawa. Currently there are 17 geothermal powerplants operational, and after a lack of interest in geothermal energy in the early 2000s, many more geothermal plants are planned after the Tohoku earthquake and nuclear disaster in 2011 (Tosha et al., 2016). Geothermal fields mainly target Quaternary volcanoes and are located in the northeast of the country on the islands of Honshu and Hokkaido (e.g. Yanaizu-Nishiyama, Kakkonda), or in the southwest in Kyushu. In the late 1980s and early 1990s two HDR test sites were drilled and stimulated at Hijiori and Ogachi, targeting granodiorite basement in calderas. Fracturing experiments at Hijiori were performed in 1998, 1992 and 1995, by injection of 1960 m^3, 51,500 m^3 and 2115 m^3 respectively (Sasaki & Kaieda, 2002). Circulation tests were performed in 1995 and 2000–2002 with recovery factors of 39% and 53% (Kaieda, 2015). At Ogachi two fracturing experiments were conducted in 1991 and 1992, injecting 10,000 m^3 and 5500 m^3 respectively (Ito, 2003; Kaieda et al., 2005; Kaieda, 2015).

At Yanaizu–Nishiyama (Okuaizu) geothermal field, seismicity was monitored by a local network ($M_c \sim 1.0$) (Asanuma et al., 2011; Mitsumori et al., 2012). Several $M > 3.0$ events occurred in the field, including a M_{JMA} 4.9 event in November 2009, after 14 years of production and reinjection. Natural seismicity also occurs in the field, but a correlation with injection has been observed (Asanuma et al., 2014). Events up to M 2.0 were recorded during fracturing at Ogachi (Kaieda et al., 2005; Kaieda, 2015), but event sizes at Hijiori did not exceed M 0.6 during the different fracturing tests (Sasaki & Kaieda, 2002). However, three months after the long-term circulation test in 2000–2002, a M 2.4 event occurred, at the edge of the stimulated reservoir (Kaieda, 2015).

Other: Other case histories included in the review include geothermal fields in Mexico and El Salvador. The largest event associated with one of these fields is M_L 6.6 which occurred on the Imperial Valley Fault in the Salton Trough (Glowacka & Nava, 1996). Large-scale production from the nearby Cerro Prieto field in Mexico caused a reduction in pressure and subsidence over a large area surrounding the field (Glowacka et al., 1999; Trugman et al., 2014). The poroelastic stress-changes and differential subsidence may have contributed to the occurrence of the M_L 6.6 event (Glowacka & Nava, 1996). Other fields in Mexico in the Mexican Volcanic Belt and Baja California (Prol-Ledesma & Morán-Zenteno, 2019) include Los Humeros (Lermo et al., 2008; Urban & Lermo, 2012, 2013; Flores-Armenta, 2014), Los Azufres (Iglesias et al., 1987; Arellano et al., 2005; Urban & Lermo, 2012), and Los Tres Virgenes (Verma et al., 2006; Antayhua-Vera et al., 2015; Prol-Ledesma et al., 2016). At Los Humeros, only a small fraction of the extracted fluid is reinjected, at Los Azufres about 50% is reinjected and at Los Tres Virgenes almost 80% is reinjected. Maximum observed magnitudes in these fields are M_d 2.5, M_d 4.6 and M_d 1.9 respectively. In El Salvador, electricity is generated at two geothermal fields: the Chipilapa–Ahuachapan (Fabriol & Beauce, 1997; Monterrosa & López, 2010) and Berlín (Rivas et al., 2005; Rodríguez & Aníbal, 2005; Kwiatek et al., 2014) fields. Maximum magnitudes detected were M_d 3.0 and M_w 3.7 (M_L 4.4) respectively. The largest event in Berlín followed a hydraulic stimulation of one of the injection wells in the field (Kwiatek et al., 2014). At the Mirvalles field in Costa Rica microseismicity increased over time, with a maximum magnitude of M_L 3.8 in 2003 (Moya & Nietzen, 2010; Moya & Taylor, 2010). At the Palinpinon geothermal field in the Philippines, seismicity up to M 2.4 was observed after starting production and injection in 1983 (Bromley et al., 1987).

Summary

The occurrence of seismic events with $M_{max} > 2.0$ for the different geothermal plays and systems discussed above is summarised in Figure 8. Most seismic events have been observed in the convection-dominated play types, mostly in the VFT and EDT (Fig. 8A). In these settings mostly hydrothermal systems (HS) are found, as well as some petrothermal systems (PS), which both show a relatively high number of $M > 2.0$ sites (Fig. 8B). Fewer events have been observed in conduction-dominated plays (IBT, OBT and BT). In particular for IBT no events of $M > 2.0$ have been reported to date. Seismicity was also mostly associated with projects targeting crystalline or metamorphic rocks (Fig. 8c). However, as observed from the review, PS in granite does not always induce $M > 2.0$ events; e.g. at Jolokia, Rittershoften and Helsinki, magnitudes did not exceed 1.9. Hot sedimentary aquifers (HSA) are only occasionally associated with seismicity of $M > 2.0$. The three cases of seismicity in HSA shown in Figure 8C are from the Molasse Basin where the underlying basement was reactivated. Operations in sandstone were not associated with a large number of $M > 2.0$ events. For HSA systems in sandstones, no $M > 2.0$ seismicity was reported, but for PS in Paralana, and HS in Mexico and USA, seismicity occurred. For the latter two cases magnitudes exceeded M 5.0.

Key factors and relation with the occurrence of felt induced events

In this section we summarise the key parameters related to the occurrence of felt induced events. The occurrence of induced seismicity is controlled by the combination of geological parameters (e.g. rock type) and operational parameters (e.g. injection pressure) obtained from the case study review. Note that it is challenging to determine unequivocal correlations between these parameters and
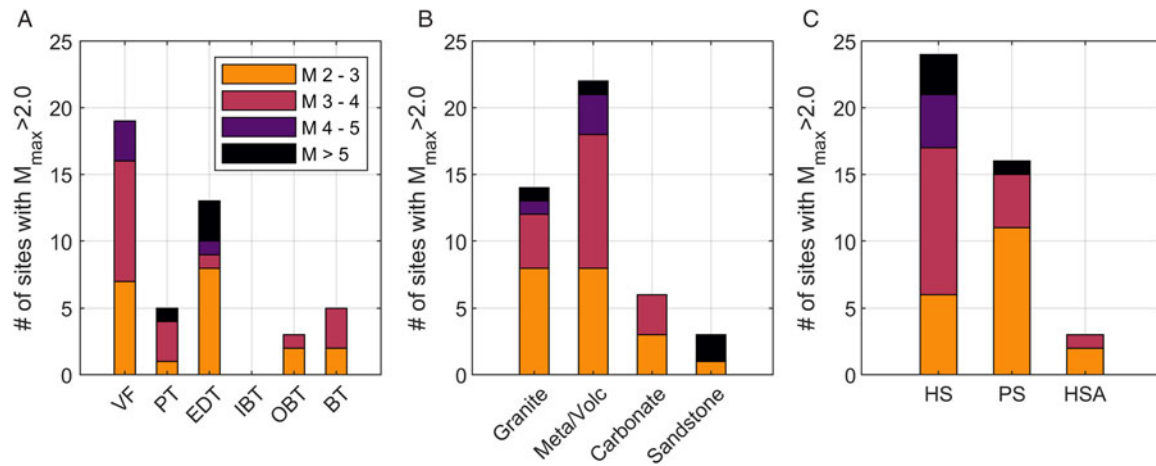
Fig. 8. Occurrence of induced seismic events for different (A) play types, with VF: volcanic fields, PT: plutonic type, EDT: extensional domain type, IBT: intracratonic basin type, OBT: orogenic belt type, and BT: basement type. (B) Rock types, and (C) system types, with PS: petrothermal systems or EGS, GF: geothermal field, and HSA: hot sedimentary aquifer.

maximum recorded magnitudes, because the parameters are often interrelated (e.g. depth and temperature) and many factors together contribute to the occurrence of felt seismicity. The following analysis attempts to establish rough trends or bounds between maximum observed earthquake magnitudes and operational or geological parameters.

Effect of geological parameters

For the cases presented in this study, felt seismicity in conduction-dominated settings only occurred in projects targeting rocks with low matrix porosity at depths larger than 2.5 km (Fig. 9A). The largest magnitude, of M 3.7, occurred due to stimulation of the Habanero EGS in the granite basement of the Cooper Basin (#2 in Fig. 9A). Also a few of the projects in the fractured carbonate rocks of the Molasse Basin generated seismicity, for example at Sankt Gallen (M_L 3.5, #23), Unterhaching (M_L 2.4, #26) and Poing (M_L 2.1, #21). Proximity and a hydraulic connection to the granitic basement resulted in seismic events in these cases. However, for most of the fractured carbonates of the Molasse Basin no seismicity was reported, even though operations (circulation) are similar. This underlines how induced seismicity can be site-specific. Also, deep and tight sandstones of the North German Basin that were hydraulically fractured did not produce felt events. Felt seismicity was also not observed for the 35 doublets targeting the relatively porous Dogger carbonates in the Paris Basin (#45) which have been operational for >30 years. Shallow porous sandstone aquifers in the North German Basin (#35–39), Norwegian–Danish Basin and in the Netherlands (WNB) have also not been associated with felt seismicity.

Felt seismicity was more often observed in geothermal projects in convection-dominated settings in tectonically active areas (Fig. 9B), in agreement with Figure 8A. Here, felt seismicity occurred in petrothermal systems (e.g. EGS projects) targeting low-porosity rocks, as well as in hydrothermal fields. The EGS projects targeted naturally fractured granites with low matrix porosity at depths > 3.0 km, including projects at Soultz-sous-Forêts (M_L 2.9) and Basel (M_L 3.4). The largest event was observed at the EGS near Pohang (M_w 5.5, #46). The geothermal fields were located at shallower depths than the EGS, with maximum depths between 2 and 3 km. The rock types and porosities vary; some

rocks such as the ignimbrites in the Taupo Volcanic Zone have a high porosity, whereas metamorphic rocks have lower porosities. Seismicity is common, and often clusters around reinjection wells (e.g. Rotokawa, the Geysers, Larderello, Hellisheiði). The largest event occurred in the Salton Sea geothermal field (M 5.5) which is composed of hydrothermally altered sandstones (#60), and at the Geysers (M 5.0, #7). The occurrence of natural seismicity sometimes makes it difficult to distinguish natural and induced seismicity, as for example at Salton Sea. Although seismicity is common, it is not always of large ($M > 4$) magnitude.

Figure 10 shows the maximum induced magnitudes against various geological parameters. Most felt induced events occurred in areas which were tectonically active (Fig. 10A), in agreement with Figure 9. All $M > 4.0$ events occurred in regions with a strain rate of 5 nanostrains a^{-1} or more. However, no further trend between the tectonic loading rates and maximum magnitudes was observed. The M_w 5.5 at the Pohang EGS (#46) occurred in an area with relatively low tectonic loading rates of ~5–6 nanostrains a^{-1}, which is more than three orders of magnitude lower than the strain rate magnitude at e.g. the Geysers (M 5.0, #7) and Salton Sea (M 5.1, #60). Projects in tectonically inactive regions (R in Fig. 10A) on the other hand also generate felt events, up to a M_L 3.7 at Habanero (#2). Both at Pohand and Habanero the pre-existing faults were close to failure, indicating that low tectonic loading rates do not mean that the stress is low. Projects in tectonically active regions on the other hand do not always generate seismicity, e.g. in the Pannonian Basin. Other factors such as the lithology and operational parameters are also of influence on seismicity.

Felt events associated with petrothermal systems (PS) and hot sedimentary aquifers (HSA) showed a clear relationship with proximity to the basement (Fig. 10B). All felt events occurred at sites which targeted depths close to the basement, whereas no felt events were reported for PS and HSA targeting formations >0.5 km away from the basement. A M_L 3.5 occurred ~0.5 km below the Sankt Gallen well; here a previously undetected fault caused the pressure perturbation to migrate to depth. This shows the importance of faults as hydraulic conduits to depth. For hydrothermal systems, on the other hand, the distance to (crystalline or metamorphic) basement had no apparent influence on the occurrence of felt events. No clear trend was visible for event magnitudes and tectonic regime.
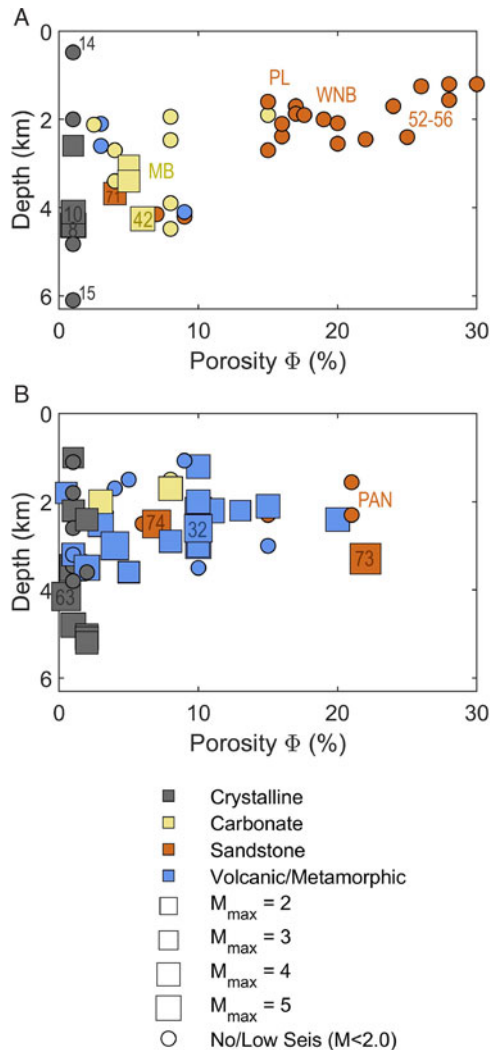
Fig. 9. Average rock matrix porosity against depth and the occurrence of induced seismicity. Cases where induced seismicity occurred are shown by square symbols where the size of the symbol scales with maximum magnitude. Cases where no seismicity was observed or seismic events were low ($M < 2.0$) are indicated with circles. Colours of the symbols give the rock type. (A) Case histories in conduction-dominated settings, including EGS and hot sedimentary aquifers (HSA). (B) Case histories in convection-dominated settings including EGS and hydrothermal systems (geothermal fields). For numbers see Table S2 (in the Supplementary Material available online at https://doi.org/10.1017/njg.2019.6); geothermal areas PL: Polish Lowlands, URG: Upper Rhine Graben, WNB: West Netherlands Basin.

Effect of operational parameters

For PS and HSA the maximum magnitudes of induced seismicity increased with the injection pressure ΔP at the wellhead (Fig. 11A). Note, however, that ΔP is closely linked to the rock type targeted for the geothermal operations. Porous sandstones and permeable carbonates are targeted in HSA, which require relatively low ΔP, generally <5 MPa. Granites targeted by EGS on the other hand require >10 MPa during stimulation. Most felt events occurred at $\Delta P > 5$ MPa, in systems targeting crystalline rock. However, seismicity was also induced at low ΔP (<1.5 MPa) during circulation at the aforementioned HSA systems at Unterhaching and Poing, as well as at Insheim in the Upper Rhine Graben. In all these cases, circulation occurred close to the crystalline basement, and most seismicity was located within the (critically stressed) basement rather than the sedimentary formation (Megies & Wassermann,

2014; Küperkoch et al., 2018). Both the magnitude of the pressure change, as well as the rock type and *in situ* stress, are thus important for the occurrence of felt events. For hydrothermal systems the relation with ΔP and induced magnitudes is not obvious. Note that e.g. at the Geysers no injection pressure is required; the reservoir formation is underpressured and water can be injected under gravity drive (here shown as ΔP 0.1 MPa). However, at the reservoir level the pressure change with respect to the initial formation pressure may be larger due to the water column, e.g. 7 MPa which is an excess pressure of ∼3.5 MPa (Martínez-Garzón et al., 2014). For future studies we recommend taking the pressure difference with respect to the initial reservoir pressure, rather than the wellhead pressure (the latter is equal to the former in case of a hydrostatic pressure gradient, but not for underpressured or overpressured reservoirs).

There was no clear correlation of $M > 2.0$ events with the absolute volume change in the geothermal systems (Fig. 11B). However, most $M > 4.0$ events occurred in hydrothermal systems in which large volume changes (often depletion) occur. One exception is the M_w 5.5 Pohang event, in which the net injected volume was ∼6000 m³, which was comparable to the volume change of other EGS. Some hot sedimentary aquifers have large volume change but no reported seismicity (dotted lines), further illustrating the lack of a clear correlation between volume change and felt seismicity. For injection-induced seismicity in general, such a correlation was observed (McGarr, 2014; Zang et al., 2014); perhaps here the range of volume changes is too limited to clearly see that correlation.

In this study, all events with $M > 2.0$ occurred in systems targeting formations of ∼100 °C and hotter (Fig. 11C and D). Temperature differences are in excess of 80 °C, up to more than 200 °C in hydrothermal systems. The data indicate a trend of increasing maximum magnitudes with increasing temperature (and in most cases associated ΔT). Again, the M_w 5.5 Pohang event is an outlier to that trend, i.e. it occurred at relatively low temperatures compared to the other sites.

Discussion

The review of the 85 geothermal case histories showed how the occurrence of induced seismicity varied for the different geothermal plays and systems analysed. The majority of felt seismic events occurred in geothermal systems in tectonically active, convection-dominated settings, both in hydrothermal systems and petrothermal systems (EGS). Also petrothermal systems in tectonically inactive regions generated felt seismicity. Hot sedimentary aquifers in tectonically inactive, conduction-dominated settings, on the other hand, mostly did not generate felt seismicity, unless operations occurred close to competent (crystalline) basement rocks. These observations provide an indication of the seismogenic potential of geothermal systems, i.e. what conditions are more or less prone to the occurrence of felt seismicity. In the following subsection we discuss the causes of different responses of geothermal reservoirs to geothermal operations. We then discuss the implications for geothermal systems in the Netherlands.

Response of geothermal reservoirs to geothermal operations

Critically stressed faults (or potentially active faults) play an important role in the occurrence of felt induced seismicity. These faults can be reactivated by small (<1 MPa) stress changes. A prominent example of this is the M_w 5.5 earthquake at the Pohang EGS site on 15 November 2017, two months after the last stimulation.
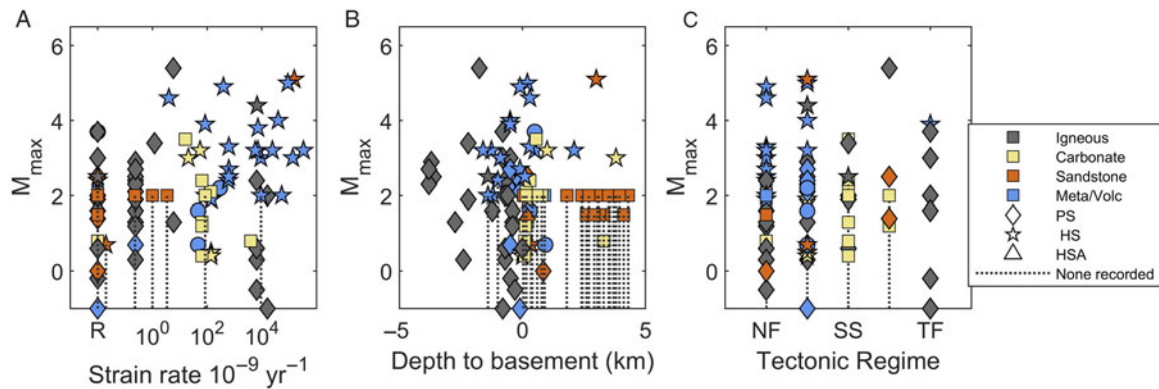
Fig. 10. Geological and tectonic parameters against maximum magnitudes observed at geothermal sites. Colours indicate the rock type of the geothermal target formation, the symbols the system type. The dotted lines indicate the range of possible magnitudes for cases where no seismicity was reported. The upper bound of this range indicated the magnitude of completeness in case local networks were present, or a *M* 2.0 (approximately the threshold for events to be felt) if no local network was present. (A) Depth to (crystalline) basement (negative values mean below basement). (B) Strain rate magnitude (second invariant of the strain rate tensor) from the Global Strain Rate Model (GSRM) (Kreemer et al., 2014). R indicates the geothermal site was situated in a region assumed inactive in the GSRM. (C) Tectonic regime, where NF: normal faulting regime, NF-SS: transtensional regime, SS: strike-slip regime, SS-TF: transpressive regime, TF: thrust faulting regime.

Although the maximum wellhead pressures reached 27 MPa during this stimulation, and almost 90 MPa during an earlier stimulation in 2016, modelling suggested that pressure diffusion caused a pressure change at the hypocentre location of only 0.07 MPa (Ge et al., 2019). However, this pressure change was enough to trigger foreshocks and the mainshock on the previously unmapped, critically stressed fault, releasing mainly tectonic strain. The seismic moment exceeded the expected moment based on the net injected volume by three orders of magnitude (Grigoli et al., 2018), again indicative of a large contribution of tectonic strain energy. Note that critically stressed faults and fractures may be present even though tectonic loading rates are low, as shown by, for example, *in situ* stress measurements in intraplate areas (Zoback & Townend, 2001) and measurements at the Fjällbacka HDR site in the Fennoscandian shield (Jupe et al., 1992). Critically stressed faults also were reactivated at, for example, Habanero in the Cooper Basin (Holl & Barton, 2015) where natural seismicity rates are low. Tectonic loading rates near Pohang were also relatively low, with little natural seismicity, although some active faults are present in the region (Ge et al., 2019). To avoid large-magnitude events it is therefore important to stay away from these critically stressed faults (see also recommendations in e.g. Baisch et al., 2016; Wiemer et al., 2017).

The review showed that the crystalline basement was prone to hosting induced events with *M* > 2.0, in agreement with previous studies (Evans et al., 2012). Critically stressed faults are often found in the basement (see previous paragraph). Furthermore, because of the impermeable nature of crystalline rocks, geothermal operations in the crystalline basement require stimulations at Δ*P* often exceeding 10 MPa, which can also reactivate less critically stressed faults and fractures near the well. Crystalline rocks are also very competent (e.g. high Young's modulus and shear modulus), and thus poroelastic and thermoelastic stress changes can be large. In addition, laboratory experiments showed granite has seismogenic frictional properties (Blanpied et al., 1995; Ge et al., 2019). However, the characteristics of the local structural fabric (fractures, faults) also play an important role in whether large-magnitude events occur. During EGS stimulations in Helsinki for example it was also noted that seismicity occurred in a 3-D ellipsoidal volume, in contrast to a planar fault structure as observed in Basel and the Cooper Basin (Kwiatek et al., 2019). Event magnitudes scaled with injected volume, so that injection strategy could be adjusted

during stimulations and magnitudes remained limited to M_w 1.9. A relatively large amount of small-scale seismic activity may have relaxed the stresses during stimulation.

Not only stimulations within the basement itself generated seismicity of *M* > 2.0; also stimulation or circulation close to the basement resulted in *M* > 2.0 events. This includes circulation in the faulted and fractured Malm carbonates in the Molasse Basin at Unterhaching and Poing, and at the transition from tight sedimentary formation to basement in the Upper Rhine Graben at Insheim and Landau (Megies & Wassermann, 2014; Küperkoch et al., 2018; LIAG, 2018). The majority of the seismic events occurred in the crystalline basement, although some may also have occurred in the tight sedimentary rocks overlying the basement (Küperkoch et al., 2018). Fractures and faults can transmit pressure changes from the well to critically stressed faults in the basement, showing how a hydraulic connection to the basement increases the seismogenic potential. This is similar to induced seismicity associated with other activities such as waste water injection, where low-pressure changes over a large area reactivated critically stressed basement faults (e.g. Zhang et al., 2013; Yeck et al., 2016). However, in the Molasse Basin the majority of geothermal systems did not generate seismicity or only generated low-magnitude events. Analysis of fault criticality showed many faults are not critical so that reactivation did not occur or only after significant thermal and chemical changes, indicating again the importance of the local structural fabric, the related hydrogeology and potential hydraulic connection to the basement, and the stress field (Seithel et al., 2019). Note that experiences from hydraulic fracturing also show that not only basement is prone to hosting felt seismic events, but highly stressed competent sedimentary formations also can host significant seismicity (Lei et al., 2019); this should be taken into account for geothermal systems as well.

Doublet operations in porous sedimentary formations did not generate felt seismicity. Both operational and geological parameters in these sedimentary formations are less likely to lead to felt seismicity. First of all, stress changes in these formations are smaller, as (re)injection pressures are low (<2 MPa), net volume changes are often zero (circulation) or negative (depletion) and the rocks themselves are less competent (in particular, poorly consolidated sands) which reduces the magnitude of poroelastic and thermoelastic stresses. In addition, the state of stress in sedimentary formations can be less critical than in the crystalline basement,
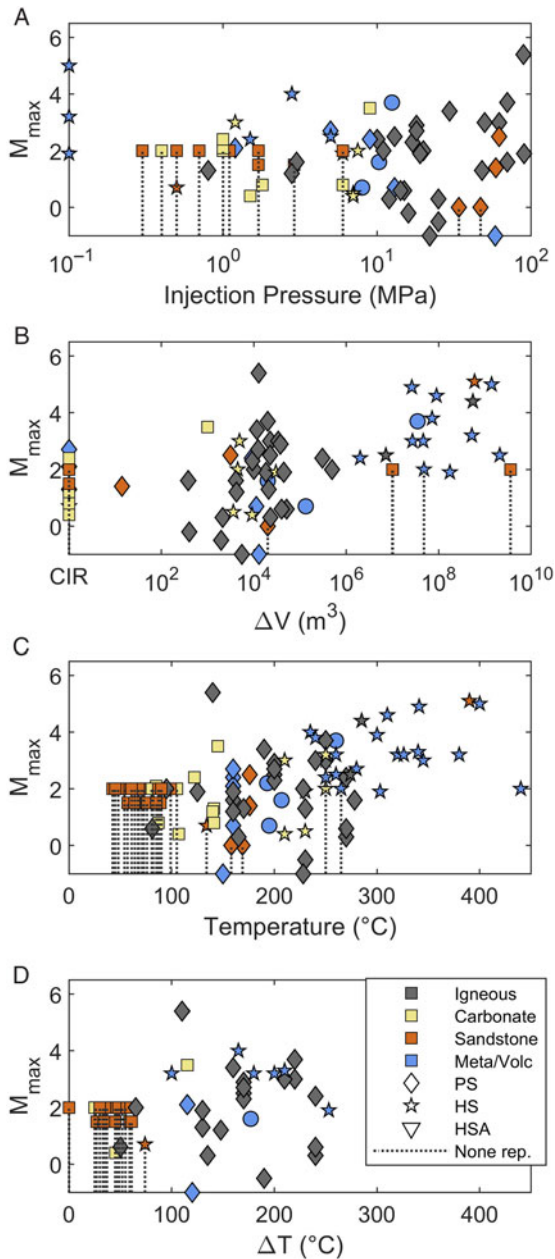
Fig. 11. Operational parameters and maximum magnitudes of induced seismicity at the sites included in the case study review. The dotted lines indicate the range of possible magnitudes for cases where no seismicity was reported. The upper bound of this range indicated the magnitude of completeness in case local networks were present, or a *M* 2.0 (approximately the threshold for events to be felt) if no local network was present. (A) Injection pressure at the wellhead, (B) Absolute volume change, (C) Maximum reservoir temperature, (D) Temperature difference between reservoir temperature and injected fluid temperature.

depending on the lithology. For example, in clay-rich formations viscoelastic creep is expected to relax a large fraction of the differential stress imposed by tectonic loading (Sone & Zoback, 2014). High σ_h/σ_v ratios (close to 1, meaning isotropic stress state) were observed in clay-rich layers, salt formations and anhydrite-rich layers, whereas in limestone layers the differential stress was much higher (Cornet & Röckel, 2012). These stable stresses in clay-rich layers would prevent an earthquake growing very large on a fault cross-cutting a succession of, for example, sands and clay-rich layers. A near-isotropic stress state in sedimentary layers around

salt domes can explain why in hydraulic fracturing tests in tight sandstones the North German Basin did not induce any (micro) seismicity, even though the maximum injection pressures reached 90 MPa (Rioseco et al., 2013). Hence, whereas stress magnitudes and directions are on average more continuous and critical in the crystalline basement, the magnitude and direction of stress in sedimentary formations can vary with depth and location, depending on the lithologies present. Another effect of the presence of clay-rich formations is that they act as an aquitard (as long as no major fault zones are present), preventing pressure change from migrating to critically stressed faults in the basement. The thick sequence of shales present between the carbonates and the crystalline basement in the Paris Basin could have prevented pressure and temperature perturbations extending to depth, and may together with the operational parameters and *in situ* stress explain why no seismicity was observed in any of the 34 doublets.

Geothermal fields which are always situated in tectonically active settings are also often seismogenic, although magnitudes are not always large. The largest magnitudes occurred in the Geysers, Salton Sea, Yanaizu Nishiyama and Hellisheidi. Often (but not always) events show a spatiotemporal correlation to reinjection operations, and thermoelastic stressing may play a large role. In Iceland for example the injectivity depended strongly on injected fluid temperature, because of increased thermal contraction of the reservoir faults and fractures with cooler fluids. It is unclear why events in some geothermal fields remain smaller than in other fields. Often subsidence is observed above the fields, in particular when the net volume depletion is large. Subsidence can be significant and contribute to inducing to seismic events, e.g. at the Geysers and Cerro Prieto. At the Cerro Prieto field the subsidence reached much further than the field boundaries, as the geothermal reservoir (sands and shales) is recharged from the sides (Glowacka et al., 1999). The large subsidence bowl interacted with several major active faults, and subsidence could have altered the stresses and triggered large earthquakes. This shows how volumetric changes due to reservoir depletion also play a role in inducing seismic events.

To summarise, interaction of operational parameters with the *in situ* state of stress and presence of large optimally oriented faults, and the hydrogeological and mechanical (i.e. rock competency, rock creep behaviour, and fault friction) properties of reservoir rocks and overburden and underburden, all have a large effect on the occurrence of *M* > 2.0 seismicity. Seismicity with *M* > 2.0 becomes more likely when operations cause stress changes on critically stressed faults (which are often found in the crystalline basement), or when stress perturbations are transmitted from sedimentary formations to the crystalline basement, e.g. if a hydraulic connection exists. The larger the pressure and temperature perturbations and the area over which they act, the larger is the chance of affecting a critically stressed fault or bringing a fault to failure. Operations in porous sandstone aquifers interbedded with clay-rich layers far from the basement are less likely to generate felt seismic events as pressure changes are lower and a hydraulic connection to the basement is often less likely (depending on the local geology). Thermoelastic stresses may, however, still be significant, and research into the response of porous sandstone formations to thermal stresses is recommended.

Relative importance of geological parameters on the occurrence of seismicity

The relative importance of the geological factors can be quantified using logistic regression (Pawley et al., 2018). Here we used logistic
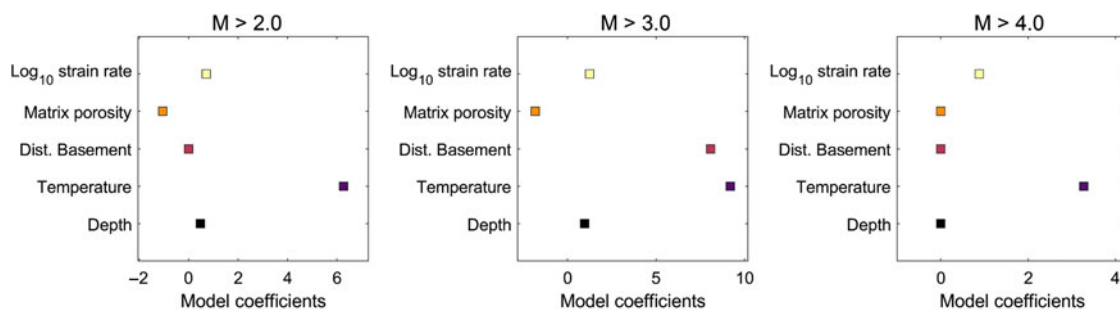
Fig. 12. Model coefficients of the logistic regression analysis of the five geological parameters on the occurrence of felt seismicity.

regression to obtain a first-order assessment of the statistical importance of geological parameters, and which parameter may be indicative of the potential for causing seismic events. The relative importance of the depth, temperature, distance to basement, matrix porosity, and logarithm of the tectonic strain rate were analysed with logistic regression with L1 regularisation in MATLAB®, with eightfold cross-validation. Strain rates of areas outside of actively deforming regions were set to 10^{-11} a^{-1}, in agreement with typical values for cratons and intraplate regions. The effect of these geological parameters on whether a site is 'seismic' (i.e. $M > 2.0$ recorded) or 'low-seismic' ($M < 2.0$ or none recorded) was investigated. We also tested two different cut-off values for seismic cases ($M > 3.0$ and $M > 4.0$). The regression was applied to all cases included in the review for which the five parameters were known. The five parameters were normalised to span a range from 0 to 1.

The L1 regressions showed that all five parameters help to explain the observed variability in seismic response (Fig. 12). For a cut-off $M > 2.0$ geothermal reservoir, temperature had the strongest influence and was positively correlated to the occurrence of seismicity. A smaller effect was observed for porosity and strain rate, that had the same strength but opposite sign (i.e. matrix porosity was negatively correlated to the occurrence of seismicity). Depth had the smallest model coefficients. For $M > 3.0$, again reservoir temperature had the strongest correlation, now followed by distance to basement. For $M > 4.0$, temperature remained strongest, followed by strain rate.

This is in agreement with the dominant mechanisms and key observations discussed in the previous subsection. Most $M > 4.0$ events were observed in geothermal fields which are situated in high-temperature and tectonically active (high strain-rate) regions. For $M > 2.0$ events the distance to basement did not show up as a dominant factor, although it was observed that operations within or close to basement were prone to generate seismicity. It was, however, also observed that the local structural fabric may have a large role in causing felt seismic events; this factor is not included in the importance analysis and could explain why basement was not a dominant factor. Also, for geothermal fields the (role of) basement is different compared to sedimentary aquifers close to basement.

As more and more geothermal projects start and knowledge increases, we recommend future work on (region-specific) logistic regression and its potential to quantify the likelihood of the occurrence of felt seismic events. In addition, if possible the presence of large faults in the vicinity of the geothermal systems and the state of stress on these faults could be included.

Implications for geothermal systems in the Netherlands

Most Dutch geothermal targets are situated in the West Netherlands Basin (WNB), which is an inactive rift basin at the west end of the Ruhr Valley Graben (RVG), or in the Central Netherlands Basin

(CNB) and the Texel–IJsselmeer High (TIJH) (Fig. 1). The target formations in these region are porous sandstone aquifers of Lower Cretaceous, Upper Jurassic or Permian age (Table 1). Other targets include fractured limestones that are found locally, e.g. in the south and southeast of the Netherlands near the Ruhr Valley Graben. Here we discuss the main geological and operational characteristics of (future) geothermal systems in the Netherlands. We relate these characteristics to the mechanisms and key factors related to the occurrence of felt seismic events, and classify the seismogenic potential for each target. The seismogenic potential is based on the key factors, as well as previous occurrences of seismicity in the geothermal target or an analogous setting in another country.

Doublet operations in the Netherlands

For geothermal doublets in the Netherlands the pumping pressure applied for the thermal loop (production plus injection) is in the order of 20% of reservoir hydrostatic pressure, due to performance and safety constraints (Van Wees et al., 2012). The allowed pressure changes at the injector are restricted to 13.5 MPa km^{-1} (State Supervision of Mines & TNO-AGE, 2013). For a saline water gradient of 10.8 MPa km^{-1} and a reservoir depth of 2 km this would, for example, give a pressure difference of 5.4 MPa at the reservoir level. For high-porous matrix-dominated reservoirs at a few hundred metres from the well, the pressure changes are likely to be small, in the order of <0.1 MPa (Willems et al., 2017). However, temperature changes can be significant; simulations of a doublet in the West Netherlands Basin show how the aquifer temperature around the injection well can decrease by more than 30 °C within an area of several hundreds of metres over 30 years (Willems et al., 2017). Such changes can cause considerable thermoelastic stressing in the cooled reservoir-volume surrounding the injection well (see 'Stress changes: thermoelastic stressing' above). The thermal stress effect is strongly dependent on thermal cooling (ΔT) and the Young's modulus (E) of rocks (Equation 1), and may thus be stronger with depth (higher ΔT and more competent rocks). Further research on the effect of thermal stresses on the potential for fault reactivation is recommended: for example on the spatiotemporal distribution of the stress changes and the stress path, and to what extent these stresses may be transmitted to or relaxed by inelastic deformation of over- and underlying clays.

In many of the geothermal regions in the Netherlands the seismic network has a magnitude of completeness of 1.5 (Dost et al., 2012). Locally the detection completeness can be lower, in particular in the north of the Netherlands near the Groningen gas field.

In the following subsections the main geothermal target formations in the Netherlands are described. For information on the nomenclature and lithological descriptions see also www.dino-loket.nl.

Table 1. Main geothermal target formations in the Netherlands and seismogenic potential. For a more extensive description of the lithostratigraphy see www.dino-loket

Age	Group	Target formation	Depth	T	Description	# of doublets[a]	Seismicity?	Analogue region from review?	Key factors	Seismogenic potential
Tertiary	Lower North Sea Group		0.4–1 (WNB)	20–45 (WNB)	Unconsolidated sediments of the Middle & Lower North Sea Group. Alternation of sandstones and clays.	0 (1 drilled)	No	Pannonian Basin	ΔP: low ΔT: ~20–50 Stress: stable? Far from basement	low
Lower Cretaceous	Rijnland Group	Vlieland Sandstone Formation	1–2.5 (WNB)	35–80 (WNB)	e.g. Berkel Sandstone Member. Sandstones with thin intercalated claystone beds.	9	No	North German Basin, Norwegian–Danish Basin, Polish Lowlands → no seismicity reported	ΔP: low ΔT: ~20–50 Stress: stable? Far from basement	low
Upper Jurassic	Schieland Group	Nieuwerkerk Formation	0.5–2.6 (WNB)	30–95 (WNB)	Alblasserdam Member, Delft Sandstone Member. Alternation of claystones and fluvial sandstones.	''	No	North German Basin, Norwegian–Danish Basin, Polish Lowlands → no seismicity reported	ΔP: low ΔT: ~20–50 Stress: stable? Far from basement	low
Lower Triassic	Main Buntsandstein Group	Hardegsen Formation Detfurth Formation Volpriehausen Formation Lower Buntsandstein Formation	2–4.5 (WNB)	75–130 (WNB)	e.g. Nederweert Sandstone Member. Alternation of anhydrite-rich sandstones and silty claystones.	1	No	North German Basin, Norwegian–Danish Basin, Polish Lowlands → no seismicity reported	ΔP: low ΔT: ~20–50 Far from basement	low
Permian	Upper Rotliegend Group	Slochteren Formation	1.5–3 (CNNLD)	60–110 (CNNLD)	Porous aeolian and fluvial sandstones. Main reservoir rock of gas fields in the Netherlands.	8	No	North German Basin, Norwegian–Danish Basin, Polish Lowlands → no seismicity reported	ΔP: low ΔT: ~20–50 Stress: stable Permian sandstone can be seismogenic for gas depletion Far from basement	low-medium
Upper Carboniferous	Limburg Group	Hunze & Dinkel Subgroups	1.5–5	30–140	Sand bodies in the Hunze and Dinkel Subgroups.	0	No			low-medium
Lower Carboniferous (Dinantian)	Carboniferous Limestone Group	Zeeland Formation	1.5–3 (RVG)	70–90 (RVG)	Karstified and/or fractured limestones.	2 (suspended)	Maybe (M1.7 recorded near doublets)	Molasse Basin (except no crystalline basement present below the Carboniferous in the Netherlands) Balmat Belgium, M_L 2.1 recorded	ΔP: low ΔT: ~20–50 Tectonically active region Carbonates prone to seismicity	medium

[a]As of 1 June 2019.
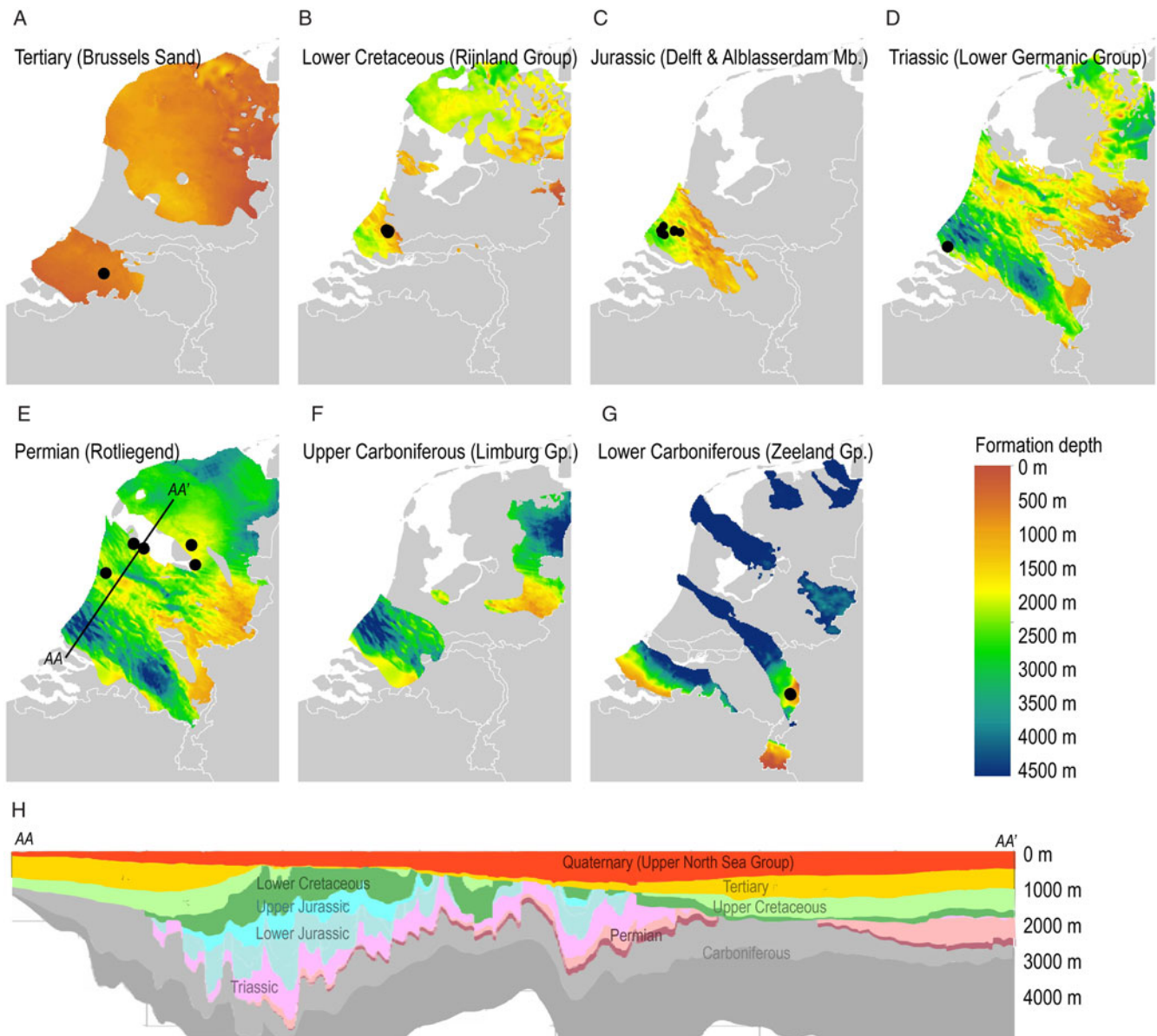
Fig. 13. Depth maps of the main geothermal target formations in the Netherlands; doublets targeting these formations are indicated by black dots. Depth maps of the aquifers are from ThermoGIS v2.1. (A) Tertiary (Brussels Formation), (B) Lower Cretaceous (Rijnland Group), (C) Upper Jurassic (Schieland Group, Delft and Alblasserdam Members), (D) Lower Triassic, (E) Permian (Rotliegend), (F) Upper Carbonfeorus (Limburg Group, Hunze and Dinkel Subgroups), (G) Lower Carbonfierous (Zeeland Group), (H) cross-section along the AA–AA′ line shown in (E) (www.dino-loket.nl).

Tertiary

Tertiary rocks (Palaeogene, Neogene) occur nearly everywhere in the Netherlands at depths of 0–1300 m, though in the RVG the depth increases locally up to 1.8 km (Fig. 13A). The thickness is mostly up to about 100 m, but in the RVG and WNB it can increase to 200–300 m. The rocks constitute loosely consolidated sandstone, siltstone and claystone of predominantly marine origin. The Tertiary rocks unconformably overlie the Cretaceous Chalk group, and are usually unconformably overlain by the sandstones, siltstones and claystones of the Quaternary Upper North Sea Group. Due to the relatively shallow depth, the temperature of the reservoirs is also relatively low. In the past the reservoirs have not attracted much attention for geothermal exploration, but the first well into the Tertiary (Zevenbergen) was drilled in 2017 to a depth of 0.8 km, reaching a temperature of 30 °C. Production

is expected to start in 2019. The loosely consolidated sandstone and shale and clays are very porous and have a low competency, and pressure and stress changes are likely low. A hydraulic connection to competent (basement) rocks at depth is not present. Operations in similar lithologies such as in the Pannonian Basin have not generated any seismicity, and the seismogenic potential of this formation is low.

Lower Cretaceous and Upper Jurassic sandstones

The Cretaceous and Upper Jurassic sandstones are a prime target of geothermal operations in the Netherlands, and have shown favourable conditions in the WNB (Fig. 13B and C). The WNB is a small transtensional basin containing a number of NW–SE-striking half-grabens that formed during the Jurassic and Early Cretaceous (e.g. Willems, 2012).
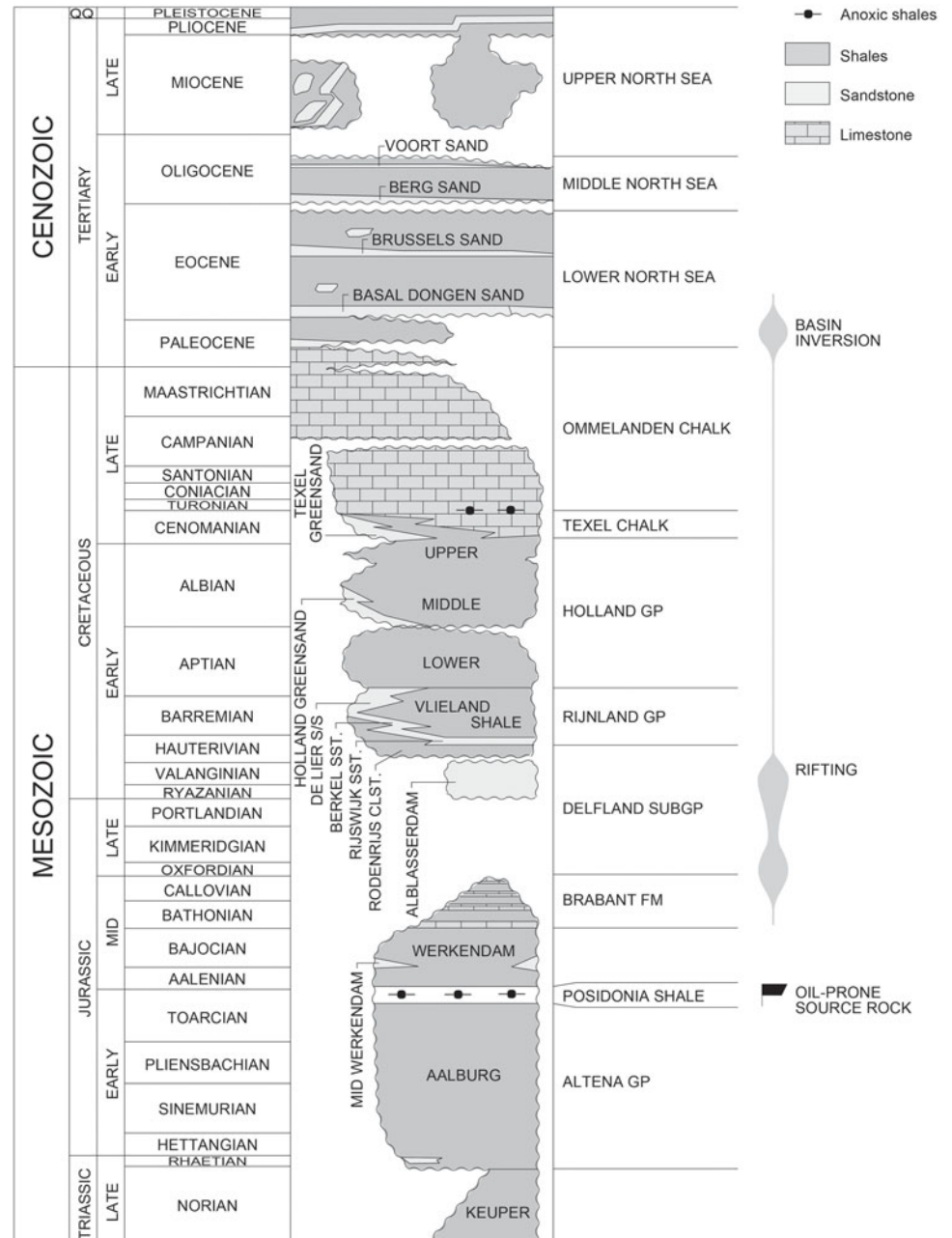
Fig. 14. Stratigraphy of the West Netherlands Basin, from the Late Triassic to the Cenozoic (DeVault & Jeremiah, 2002). AAPG©2002. Reprinted with permission of the American Association of Petroleum Geologists (AAPG) whose permission is required for further use.

The doublets drilled to these formations have reached depths of 2–3 km, reaching temperatures between 60 and 90 °C (Table S1, in the Supplementary Material available online at https://doi.org/10.1017/njg.2019.6). Figure 14 shows the stratigraphy of the WNB, including the main target formations which are the Vlieland Sandstone Formation (with the Berkel Sandstone and Rijswijk Members) and Nieuwerkerk Formation (with the Delft and Alblasserdam Members), which are comprised of fluvial sands interbedded with clay layers with average porosities of 20% (DeVault & Jeremiah, 2002, Willems, 2012; Vondrak et al., 2014; Donselaar et al., 2015). The Upper Jurassic is underlain by the Aalburg Formation of the Altena Group, which consists of calcareous claystones (www.dino-loket.nl). The presence of these thick clay-rich sequences and the depth of the basement (>5.5 km) makes a hydraulic connection to the basement unlikely.

The basin is tectonically inactive, and the stress is extensional with the maximum horizontal stress oriented NW–SE. The stress magnitudes are unknown. Several oil and gas fields targeting the Lower Cretaceous and Upper Jurassic formations are present in the area (e.g. Fig. 1B), such as the Berkel Field, De Lier Field and the IJsselmonde Field (www.nlog.nl, de Jager et al., 1996). These fields, although they are located somewhat shallower than the geothermal doublets, have not led to any induced events over decades of hydrocarbon production, suggesting the stress is not critical. Also the geothermal doublets have been operational from 2006 without inducing (felt) seismicity. In similar geological settings in the North German Basin and Poland no events have been recorded. These observations suggest that geothermal operations in the shallow porous sandstones of the West Netherlands are unlikely to generate seismicity.

Triassic sandstones

Another geothermal target formation is the Triassic Buntsandstein Group (Fig. 1D), including the Nederweert Sandstone, Volpriehausen Formation, Dethlingen Formation and Hardegsen Formation, which are comprised of a succession of sandstones and silty claystones. The Main Buntsandstein Group is underlain by a 150 m thick Lower Triassic succession of clays and sands, and overlain by evaporites, claystones and carbonates of the Upper Germanic Trias Group. The Buntsandstein Group has favourable conditions for geothermal exploitation in the WNB and possibly in the RVG in the southeast (e.g. Kramers et al. 2012), with temperatures of 75–130 °C and depths of 2–4.5 km. However, due to a burial anomaly the porosity and permeability are low in the central parts of the WNB and the RVG in the southeast. At the margins of the WNB porosity is good, ranging from 10% at 3 km to 20% at 2 km depth (Bender, 2012). Here the Vierpolders doublet (Fig. 13C) has been circulating since the start of 2016. The state of stress is unknown, but no induced seismicity has been observed in relation to geothermal operations, or in relation to oil and gas fields targeting the Buntsandstein Formation in the WNB such as the Brakel Field (www.nlog.nl). In the Brakel Field, hydraulic fracturing was performed in 2008 with injection pressure >25 MPa, but no seismicity was reported and the state of stress was likely not critical. The distance between geothermal operations in the Trias in the WNB and basement is large (>2 km) and a hydraulic connection to basement is thus unlikely. Pressure changes are low, but temperature change may be significant. In similar geological settings in the North German Basin and Poland no events have been recorded. These factors indicate that geothermal operations in the Triassic sandstones of the West Netherlands are unlikely to generate felt seismicity, but it remains important to avoid large faults. Note however that in other areas (CNB, northern Netherlands) gas production from the Buntsandstein Formation has led to felt seismic events, notably in the Roswinkel Field (up to M_L 3.4), and the offshore Q04-A field (up to M_L 2.7) and Q01-B field (up to M_L 2.6) (Fig. 1B). We recommend further research into the response of the Triassic Buntsandstein Formation to geothermally induced stress changes, and potential differences in geological and petrophysical parameters and stress between the WNB and other areas in the Netherlands.

Permian sandstones

The Permian Slochteren sandstone Formation of the Permian Rotliegend has favourable temperature–depth conditions in the CNB and TIJH. Six doublets are currently producing in the provinces of North Holland and Flevoland (Fig. 13E): the three Middenmeer doublets, Koekoekspolder (Veldkamp et al., 2015), Andijk, and Luttelgeest. These doublets target depths between 1.9 and 2.3 km where temperatures are 70–100 °C (Table S1 in the Supplementary Material available online at https://doi.org/10.1017/njg.2019.6). The Slochteren is overlain by anhydrites, carbonates and rock salt, which likely have stable stresses due to viscoelastic relaxation. Here the Upper Carboniferous underburden (Limburg Group) is composed of sands, shales and mudstones (Ruurlo Formation, www.dinoloket.nl). Seismic events have been observed for gas fields producing from Permian sandstones in the north and west of the Netherlands at a depth of 3 km. These include the Groningen gas field with >1000 earthquakes with magnitudes up to M_L 3.6, the Bergermeer field with several M_L > 3 events, the Eleveld field (up to M_L 2.8), and the Annerveen field (up to M_L 2.4). Many of these events occurred after decennia of production, which can be an indication that the state of stress is

initially not critical. The formation can be seismogenic, but the stress path and stress changes due to gas depletion are different than those in geothermal systems. We recommend further research into the differences and similarities between the stress changes generated during gas depletion and geothermal operations; in particular the thermoelastic stress which can be large. Seismogenic potential of the doublets is likely low, but care must be taken to stay away from faults (see also e.g. Baisch et al., 2016; Wiemer et al., 2017). Care must be taken also in case of geothermal activities in or near (former) gas fields, as gas depletion may have altered the state of stress.

Upper Carboniferous

A potential target formation is the Upper Carboniferous sandstone rocks of the Hunze and Dinkel Groups (Fig. 13F). These occur mainly in the east and WNB, whereas in the rest of the Netherlands the Hunze and Dinkel Group are characterised by shales. The sandstones were formed as sheet flood and fluvial channel sandstones. The aquifer is underlain by shales of the Epen Formation, and overlain by sandstones of the Rotliegend. The expected permeabilities are low, with the exception of the eastern part of the Netherlands, coinciding with a shallow depth and therefore relatively low temperature. In the largest part of the WNB, the rocks are buried too deep for conventional geothermal doublet operations without the necessity of stimulation.

Lower Carboniferous

The deepest formation currently targeted in the Netherlands is the fractured and karstified Zeeland Formation of the Carboniferous Limestone Group. In large parts of the Netherlands the Zeeland Formation lies at depth >4 km (Fig. 13F), and its composition in these parts is unknown (Fig. 13G). In the province of Limburg in the southeast of the Netherlands, karstified, fractured and faulted Dinantian limestones of the Zeeland Group are targeted by two doublets: Californië Wijnen Geothermie (CWG) which started in January 2013, and Californië Lipzig Gielen (CLG) which started in the summer of 2017 (Table S2, in the Supplementary Material available online at https://doi.org/10.1017/njg.2019.6; Burghout et al., 2019; Vörös and Baisch, 2019). The doublets are situated in a stable fault block (Peel and Venlo blocks) north of the RVG and reach a depth of ∼2.5 km (Fig. 13F). Matrix porosity is low, but permeability is provided by the fractures and faults. The production wells of both doublets, and the injection well of CWG cross-cut the Tegelen Fault, which is a large fault bounding the Venlo Block (Vörös & Baisch, 2019). Natural seismicity occurs in the region, with eight events with $M > 2.2$ within 20 km of the doublets. Slip tendency analysis indicates that the state of stress on (some) faults including the Tegelen Fault is close to failure (Vörös & Baisch, 2019). At this location the Zeeland Formation is overlain by claystones (Epen Formation), and competent Devonian sandstones/quartzites may be present in the underburden (Reith, 2018; Burghout et al., 2019).

Even though pressure changes during circulation are small, the fact that circulation occurred through a large fault zone motivated local monitoring of seismicity, which was conducted from 2014 (Baisch & Vörös, 2019; Vörös & Baisch, 2019). Operations in CWG were suspended in May 2018. After a small (M_L 0.0) event occurred near CLG in August 2018, operations were halted. Within two weeks, nine more events occurred up to M_L 1.7. Since then, operations in both doublets remained suspended because of the uncertainties related to the nature of the seismic events (State Supervision of Mines, 2019). Although the events appear

to occur several km below the geothermal reservoir (Spetzler et al., 2018; Baisch and Vörös, 2019), they are temporally correlated to production stops in the CWG doublet. A possible explanation could be the interplay between pressure changes and thermal stresses (Baisch & Vörös, 2019; Vörös & Baisch, 2019).

Doublet operations in carbonates abroad have occasionally generated seismicity with $M > 2.0$. Recently, injection tests in a geothermal well targeting the same limestone in Belgium (Balmatt) have generated events up to M_L 2.1 (23 June 2019), clearly lining up on a linear structure close to the injection well signifying that a fault has been reactivated (www.vito.be). Doublets in the Malm carbonates of the Molasse Basin near Munich have in a few instances (2 out of 16) caused induced events (M 2.0–2.4). Most of these larger events occurred in the underburden of the Malm, i.e. in the crystalline basement. This is different from the situation in the Netherlands where other (competent) sediments underlie the Lower Carboniferous Limestone instead of crystalline rocks (though stressed, competent sedimentary formations may also host seismic events). Smaller events have occurred in the vicinity of other doublets in the Malm (Seithel et al., 2019). Fault analysis showed that the occurrence of seismicity is site-specific and depends, among other things, on the structural fabric and state of stress (Seithel et al., 2019).

The observations from the Netherlands and abroad show that (small to moderate) seismic events may thus occur in or around geothermal operations in carbonate formations, and the potential for induced seismicity is larger than for the porous sandstone aquifers. It is important to characterise large faults in the vicinity of the (planned) geothermal system, and their reactivation potential in the stress field.

The review showed that geothermal operations in most geological settings comparable to those found in the Netherlands did not generate $M > 2.0$ events. However, seismicity cannot be excluded. In particular, in faulted carbonates $M > 2.0$ events may occur, but the potential for these events remains site-specific and dependent on the local fault and fracture fabric and the state of stress. Taking into account the different key parameters shown in Table 1 helps to assess the possibility of the occurrence of felt events and motivate additional characterisation of the subsurface in case the potential for $M > 2.0$ events is larger than desired. Additionally, it is also important to inform and involve the public on the development of geothermal systems and potential hazards as we proceed with the energy transition (McComas et al., 2016).

Conclusion

A case history review was performed to assess the potential for the occurrence of felt induced seismicity in geothermal systems. A total of 85 cases in various geothermal plays were analysed. Here the main findings are listed:

- The review shows that doublet operations in shallow, porous sandstone formations did not induce $M > 2.0$ seismicity. Porous sandstone layers are usually found at relatively shallow depth, and are far away from the crystalline basement which is prone to seismicity. Also the pressure changes are small as no stimulation is required. Furthermore sandstone formations are often intercalated with clay and shale layers, which could hydraulically isolate the formation from deeper layers.
- Geothermal operations within crystalline basement are prone to generate felt seismicity. Crystalline basement is competent, often critically stressed, and usually must be stimulated before fluid flow between wells can be established, i.e. larger pressure

changes. Relatively small stress changes (0.01–1 MPa) can be enough to cause induced seismicity on already critically stressed faults, as demonstrated by the Pohang earthquake. The local structural geology affects how large the induced events become, e.g. injection into a large fault zone can transmit pressure perturbation further and/or result in larger seismic events.
- Circulation in doublets or drilling operations in fractured sediments occasionally generated felt seismic events. Pressure diffusion through fractures can result in reactivation of critically stressed faults, in particular when connected to the basement. This shows a hydraulic connection to more competent formations at depth can be a potential hazard as these critically stressed faults can be encountered.
- Geothermal fields in fractured sedimentary, metamorphic and volcanic rock (hydrothermal systems) regularly generate felt seismic events. The largest events occurred in the large-size fields in the western USA and Mexico, e.g. the Geysers, Salton Sea and Cerro Prieto. These fields are associated with significant subsidence, poroelastic and thermoelastic stresses.
- In regions with high natural seismicity it can be difficult to distinguish natural and induced seismicity. For example, for some geothermal fields there are clear spatiotemporal correlations of seismicity and field operations (e.g. the Geysers, Rotokawa), but for others such a correlation is absent (e.g. Salton Sea).
- The main mechanisms for induced seismicity in geothermal systems are pore pressure increase, poroelastic stressing and thermoelastic stressing. Also, chemical changes of fault properties may play a role.
- Most felt induced events occurred in areas which were tectonically active. However, tectonic loading rates (and natural seismicity rates) are not always a good proxy for the occurrence of induced seismicity. *In situ* stresses may still be critical in areas of low loading rates. In the sedimentary cover, stresses could on the other hand be lower or more variable. Site-specific analysis of the state of stress is thus important.
- Key factors for the occurrence of $M > 2.0$ events are the presence of critically stressed faults, distance to basement and a hydraulic connection to the basement, the magnitude of pressure and temperature changes, and possibly the rock competency of target reservoir and overburden/underburden. In general, these parameters and hence the seismogenic potential increases with depth.
- Induced seismicity is always site-specific and depends on the type of operations, and can never be fully excluded. By taking into account the dominant mechanisms, the geological and operational key factors, the potential for induced events can be assessed/estimated/ categorised.

Supplementary material. Supplementary material is available online at https://doi.org/10.1017/njg.2019.6. This material comprises a table with doublets in the Netherlands (Table S1) and a table of the parameters collected for the reviewed case histories (Table S2).

References

Agemar, T., Weber, J. & Schulz, R., 2014. Deep geothermal energy production in Germany. Energies **7**(7): 4397–4416.

Albaric, J., Oye, V., Langet, N., Hasting, M., Lecomte, I., Iranpour, K., Messeiller, M., & Reid, P., 2014. Monitoring of induced seismicity during the first geothermal reservoir stimulation at Paralana, Australia. Geothermics **52**: 120–131.

Antayhua-Vera, Y., Lermo-Samaniego, J., Quintanar-Robles, L. & Campos-Enríquez, O., 2015. Seismic activity and stress tensor inversion at Las Tres Vírgenes volcanic and geothermal field (México). Journal of Volcanology and Geothermal Research **305**: 19–29.

Arellano, V.M., Torres, M.A. & Barragán, R.M., 2005. Thermodynamic evolution of the Los Azufres, Mexico, geothermal reservoir from 1982 to 2002. Geothermics **34**(5): 592–616.

Armannsson, H., 2016. The fluid geochemistry of Icelandic high temperature geothermal areas. Applied Geochemistry **66**: 14–64.

Asanuma, H., Mitsumori, S., Adachi, M., Saeki, K., Aoyama, K., Ozeki, H., Mukuhira, Y. & Niitsuma, H., 2011. Characteristics of microearthquakes at Yanaizu-Nishiyama geothermal field. GRC Transactions **35**: 989–994.

Asanuma, H., Eto, T., Adachi, M., Saeki, K., Aoyama, K., Ozeki, H. & Häring, M., 2014. Seismostatistical characterization of earthquakes from geothermal reservoirs. 39th Workshop on Geothermal Reservoir Engineering, 24–26 February 2014, Stanford, CA, USA. Conference proceedings.

Baisch, S. & Vörös, R., 2019. Earthquakes near the Californië geothermal site: August 2015–November 2018. Report No. CLGG005. Q-con GmbH (Bad Bergzabern),

Baisch, S., Weidler, R., Voros, R., Wyborn, D. & Graaf, L.d., 2006. Induced seismicity during the stimulation of a geothermal HFR reservoir in the Cooper Basin, Australia. Bulletin of the Seismological Society of America **96**(6): 2242–2256.

Baisch, S., Vörös, R., Weidler, R. & Wyborn, D., 2009. Investigation of fault mechanisms during geothermal reservoir stimulation experiments in the Cooper Basin, Australia. Bulletin of the Seismological Society of America **99**(1): 148–158.

Baisch, S., Rothert, E., Stang, H., Vörös, R., Koch, C. & McMahon, A., 2015. Continued geothermal reservoir stimulation experiments in the Cooper Basin (Australia). Bulletin of the Seismological Society of America **105**(1): 198–209.

Baisch, S., Koch, C., Stang, H., Pittens, B., Drijver, B. & Buik, N., 2016. Defining the framework for seismic hazard assessment in geothermal projects V0.1. Technical Report. Report No. 161005. KennisAgenda Aardwarmte (Bad Bergzabern).

Bálint, A. & Szanyi, J., 2015. A half century of reservoir property changes in the Szentes geothermal field, Hungary. Central European Geology **58**(1–2): 28–49.

Baria, R., Baumgartner, J., Gerard, A., Jung, R. & Garnish, J., 1999. European HDR research programme at Soultz-sous-Forêts (France). Geothermics **28**(4–5): 655–669.

Batchelor, A., 1982. Stimulation of a hot dry rock geothermal reservoir in the Cornubian granite, England. 8th Workshop on Geothermal Reservoir Engineering, 14–16 December 1982, Stanford, CA, USA. Conference proceedings.

Batini, F., Console, R. & Luongo, G., 1985. Seismological study of Larderello–Travale geothermal area. Geothermics **14**(2–3): 255–272.

Batini, F., Brogi, A., Lazzarotto, A., Liotta, D. & Pandeli, E., 2003. Geological features of Larderello-Travale and Mt. Amiata geothermal areas (southern Tuscany, Italy). Episodes **26**(3): 239–244.

Baujard, C., Genter, A., Dalmais, E., Maurer, V., Hehn, R., Rosillette, R., Vidal, J. & Schmittbuhl, J., 2017. Hydrothermal characterization of wells GRT-1 and GRT-2 in Rittershoffen, France: implications on the understanding of natural flow systems in the Rhine Graben. Geothermics **65**: 255–268.

Baumann, T., Bartels, J., Lafogler, M. & Wenderoth, F., 2017. Assessment of heat mining and hydrogeochemical reactions with data from a former geothermal injection well in the Malm Aquifer, Bavarian Molasse Basin, Germany. Geothermics **66**: 50–60.

Benato, S., Hickman, S., Davatzes, N.C., Taron, J., Spielman, P., Elsworth, D., Majer, E.L. & Boyle, K., 2016. Conceptual model and numerical analysis of the Desert Peak EGS project: reservoir response to the shallow medium flow-rate hydraulic stimulation phase. Geothermics **63**: 139–156.

Bender, A., 2012. GeoMEC-4P Geothermal Energy Brielle. Report No. G945. Panterra (Leiderdorp).

Blanpied, M.L., Lockner, D.A. & Byerlee, J.D., 1995. Frictional slip of granite at hydrothermal conditions. Journal of Geophysical Research: Solid Earth **100**(B7): 13045–13064.

Blöcher, G., Cacace, M., Jacquey, A.B., Zang, A., Heidbach, O., Hofmann, H., Kluge, C. & Zimmermann, G., 2018. Evaluating micro-seismic events triggered by reservoir operations at the geothermal site of Groß Schönebeck (Germany). Rock Mechanics and Rock Engineering **51**(10): 3265–3279.

Bönnemann, C., Schmidt, B., Ritter, J., Gestermann, N., Plenefish, T. & Wegler, U., 2010. Das seismische Ereignis bei Landau vom 15. August 2009. Abschlussbericht der Expertengruppe "Seismisches Risiko bei hydrothermaler Geothermie" (Hannover).

Braun, T., Cesca, S., Kühn, D., Martirosian-Janssen, A. & Dahm, T., 2018. Anthropogenic seismicity in Italy and its relation to tectonics: state of the art and perspectives. Anthropocene **21**: 80–94.

Breede, K., Dzebisashvili, K. & Falcone, G., 2015. Overcoming challenges in the classification of deep geothermal potential. Geothermal Energy Science **3**(1): 19–39.

Brodsky, E.E. & Lajoie, L.J., 2013. Anthropogenic seismicity rates and operational parameters at the Salton Sea Geothermal Field. Science (New York) **341**(6145): 543–546.

Bromley, C., Pearson, C. & Rigor Jr, D., 1987. Microearthquakes at the Puhagan geothermal field, Philippines: a case of induced seismicity. Journal of Volcanology and Geothermal Research **31**(3–4): 293–311.

Buijze, L., Bijsterveld, L. van, Cremer, H., Paap, B., Veldkamp, H., Wassing, B., Wees, J.D. van & Heege, J.H., 2019. Review of worldwide geothermal projects: mechanisms and occurrence of induced seismicity. Report TNO2019R100043. TNO – Geological Survey of the Netherlands (Utrecht).

Bujakowski, W. & Wojnarowski, P., 2005. Recent studies of the low Cretaceous geothermal reservoir in Mszczonów, Poland. World Geothermal Congress, 24–29 April 2005, Antalya, Turkey. Conference proceedings.

Buonasorte, G., Cameli, G.M., Fiordelisi, A., Parotto, M. & Perticone, I., 1995. Results of geothermal exploration in Central Italy (Latium–Campania). World Geothermal Congress 18–31 May 1995, Florence, Italy. Conference proceedings.

Burghout, L., Vorage, R. & Broothaers, M., 2019. Koepelnotitie Aardwarmtewinning en Seismiciteit Californie Lipzig Gielen Geothermie BV Tuinbouwgebied Californie Horst aan de Maas. Californië Lipzig Gielen Geothermie.

Cardiff, M., Lim, D.D., Patterson, J.R., Akerley, J., Spielman, P., Lopeman, J., Walsh, P., Singh, A., Foxall, W. & Wang, H.F., 2018. Geothermal production and reduced seismicity: correlation and proposed mechanism. Earth and Planetary Science Letters **482**: 470–477.

Cavarretta, G., Gianelli, G., Scandiffio, G. & Tecce, F., 1985. Evolution of the Latera geothermal system II: metamorphic, hydrothermal mineral assemblages and fluid chemistry. Journal of Volcanology and Geothermal Research **26**(3–4): 337–364.

Cant, J., Siratovich, P., Cole, J., Villeneuve, M. & Kennedy, B., 2018. Matrix permeability of reservoir rocks, Ngatamariki geothermal field, Taupo Volcanic Zone, New Zealand. Geothermal Energy **6**(1): 1–28.

Charléty, J., Cuenot, N., Dorbath, L., Dorbath, C., Haessler, H. & Frogneux, M., 2007. Large earthquakes during hydraulic stimulations at the geothermal site of Soultz-sous-Forêts. International Journal of Rock Mechanics & Mining Sciences **44**: 1091–1105.

Chen, L. & Talwani, P., 1998. Reservoir-induced seismicity in China. Pure and Applied Geophysics **153**(1): 133–149.

Cornet, F., Helm, J., Poitrenaud, H. & Etchecopar, A., 1997. Seismic and aseismic slips induced by large-scale fluid injections. In: Talebi, S. (ed.): Seismicity associated with mines, reservoirs and fluid injections. Springer (Basel): 563–583.

Cornet, F.H. & Röckel, T., 2012. Vertical stress profiles and the significance of 'stress decoupling'. Tectonophysics **581**: 193–205.

Davatzes, N.C. & Hickman, S.H., 2010. The feedback between stress, faulting, and fluid flow: lessons from the Coso Geothermal Field, CA, USA. World Geothermal Congress, 25–29 April 2010, Bali, Indonesia. Conference proceedings.

Davis, S.D., Nyffenegger, P.A. & Frohlich, C., 1995. The 9 April 1993 earthquake in south-central Texas: was it induced by fluid withdrawal? Bulletin of the Seismological Society of America **85**(6): 1888–1895.

Deichmann, N., Kraft, T. & Evans, K.F., 2014. Identification of faults activated during the stimulation of the Basel geothermal project from cluster analysis and focal mechanisms of the larger magnitude events. Geothermics **52**: 84–97.

De Jager, J., Doyle, M.A., Grantham, P.J., & Mabillard, J.E., 1996. Hydrocarbon habitat of the West Netherlands Basin. In: Geology of gas and oil under the Netherlands. Springer (Dordrecht): 191–209.

Dentzer, J., Lopez, S., Violette, S., & Bruel, D., 2016. Quantification of the impact of paleoclimates on the deep heat flux of the Paris Basin. Geothermics **61**: 35–45.

DeVault, B. & Jeremiah, J., 2002. Tectonostratigraphy of the Nieuwerkerk Formation (Delfland subgroup), west Netherlands basin. AAPG Bulletin **86**(10): 1679–1707.

Diehl, T., Kraft, T., Kissling, E. & Wiemer, S., 2017. The induced earthquake sequence related to the St. Gallen deep geothermal project (Switzerland): fault reactivation and fluid interactions imaged by microseismicity. Journal of Geophysical Research: Solid Earth **122**(9): 7272–7290.

Donselaar, M.E., Groenenberg, R.M. & Gilding, D.T., 2015. Reservoir geology and geothermal potential of the Delft Sandstone Member in the West Netherlands Basin. World Geothermal Congress, 19–25 April 2015, Melbourne, Australia. Conference proceedings.

Dorbath, L., Cuenot, N., Genter, A. & Frogneux, M., 2009. Seismic response of the fractured and faulted granite of Soultz-sous-Forêts (France) to 5 km deep massive water injections. Geophysical Journal International **117**: 653–675.

Dost, B., Goutbeek, F., Van Eck, T. & Kraaijpoel, D., 2012. Monitoring induced seismicity in the north of the Netherlands: status report 2010. Scientific Report. Report No. WR 2012-03. Royal Netherlands Meteorological Institute (De Bilt).

Eggertsson, G., Lavallée, Y., Kendrick, J. & Markússon, S., 2018. Improving fluid flow in geothermal reservoirs by thermal and mechanical stimulation: the case of Krafla volcano, Iceland. Journal of Volcanology and Geothermal Research **320**: 128–143.

Erlström, M., Boldreel, L. O., Lindstrom, S., Kristensen, L., Mathiesen, A., Andersen, M., Kamla, E. & Nielsen, L., 2018. Stratigraphy and geothermal assessment of Mesozoic sandstone reservoirs in the Oresund Basin – exemplified by well data and seismic profiles. Bulletin of the Geological Society of Denmark **66**: 123–149.

Evans, K.F., Zappone, A., Kraft, T., Deichmann, N. & Moia, F., 2012. A survey of the induced seismic responses to fluid injection in geothermal and CO_2 reservoirs in Europe. Geothermics **41**: 30–54.

Fabriol, H. & Beauce, A., 1997. Temporal and spatial distribution of local seismicity in the Chipilapa-Ahuachapán geothermal area, El Salvador. Geothermics **26**(5–6): 681–699.

Faulds, J.E., Coolbaugh, M.F., Benoit, D., Oppliger, G., Perkins, M., Moeck, I. & Drakos, P., 2010. Structural controls of geothermal activity in the northern Hot Springs Mountains, western Nevada: the tale of three geothermal systems (Brady's, Desert Peak, and Desert Queen). Geothermal Resources Council Transactions **34**: 675–683.

Flores-Armenta, M., 2014. Geothermal activity and development in Mexico: keeping the production going. Short Course VI on Utilization of Low- and Medium-Enthalpy Geothermal Resources and Financial Aspects of Utilization, organized by UNU-GTP and LaGeo, 23–29 March 2014, Santa Tecla, El Salvador.

Flóvenz, O., Ágústsson, K., Guðnason, E.Á & Kristjánsdóttir, S., 2015. Reinjection and induced seismicity in geothermal fields in Iceland. World Geothermal Congress, 19–25 April 2015, Melbourne, Australia. Conference proceedings.

Foulger, G.R., Wilson, M.P., Gluyas, J.G., Julian, B.R. & Davies, R.J., 2018. Global review of human-induced earthquakes. Earth-Science Reviews **178**: 438–514.

Franz, M., Barth, G., Zimmermann, J., Budach, I., Nowak, K. & Wolfgramm, M., 2018. Geothermal resources of the North German Basin: exploration strategy, development examples and remaining opportunities in Mesozoic hydrothermal reservoirs. Geological Society of London, Special Publication 469.

Frederiksen, S., Nielsen, S.B. & Balling, N., 2001. A numerical dynamic model for the Norwegian–Danish Basin. Tectonophysics **343**(3–4): 165–183.

Garcia, J., Hartline, C., Walters, M., Wright, M., Rutqvist, J., Dobson, P. F. & Jeanne, P., 2016. The Northwest Geysers EGS demonstration project, California: Part 1: characterization and reservoir response to injection. Geothermics **63**: 97–119.

Gaucher, E., 2016. Earthquake detection probability within a seismically quiet area: application to the Bruchsal geothermal field. Geophysical Prospecting **64**(2): 268–286.

Ge, S., Giardini, D., Ellsworth, W., Shimamoto, T. & Townend, J., 2019. Overseas Research Advisory Committee report on the Pohang earthquake. The Geological Society of Korea (Seoul).

Giovanni, B., Guido, C. & Adolfo, F., 2005. Characteristics of geothermal fields in Italy. Giornale di Geologia Applicata **1**: 247–254.

Glowacka, E. & Nava, F. A., 1996. Major earthquakes in Mexicali Valley, Mexico, and fluid extraction at Cerro Prieto Geothermal Field. Bulletin of the Seismological Society of America **86**(1A): 93–105.

Glowacka, E., González, J. & Fabriol, H., 1999. Recent vertical deformation in Mexicali Valley and its relationship with tectonics, seismicity, and the exploitation of the Cerro Prieto geothermal field, Mexico. Pure and Applied Geophysics **156**(4): 591–614.

Goldbrunner, J., 1999. Hyrdogeology of deep groundwaters in Austria. Mitteilungen der Österreichischen Geologischen Gesellschaft **92**: 281–294.

Górecki, W., Sowiżdżał, A., Hajto, M. & Wachowicz-Pyzik, A., 2015. Atlases of geothermal waters and energy resources in Poland. Environmental Earth Sciences **74**(12): 7487–7495.

Grad, M. & Polkowski, M., 2016. Seismic basement in Poland. International Journal of Earth Sciences **105**(4): 1199–1214.

Grigoli, F., Cesca, S., Rinaldi, A.P., Manconi, A., López-Comino, J.A., Clinton, J.F., Westaway, R., Cauzzi, C., Dahm, T. & Wiemer, S., 2018. The November 2017 M_w 5.5 Pohang earthquake: a possible case of induced seismicity in South Korea. Science **360**(6392): 1003–1006.

Grimmer, J.C., Ritter, J.R.R., Eisbacher, G.H. & Fielitz, W., 2017. The Late Variscan control on the location and asymmetry of the Upper Rhine Graben. International Journal of Earth Sciences **106**(3): 827–853.

Häring, M.O., Schanz, U., Ladner, F. & Dyer, B.C., 2008. Characterisation of the Basel 1 enhanced geothermal system. Geothermics **37**: 469–495.

Henrys, S. & Hochstein, M., 1990. Geophysical structure of the Broadlandsohaaki geothermal field (New Zealand). Geothermics **19**(2): 129–150.

Hjuler, M.L., Vosgerau, H., Nielsen, C.M., Frykman, P., Kristensen, L., Mathiesen, A., Bidstrup, T. & Nielsen, L.H., 2014. A multidisciplinary study of a geothermal reservoir below Thisted, Denmark. Geological Survey of Denmark and Greenland Bulletin **31**: 51–54.

Holl, H. & Barton, C., 2015. Habanero Field:– structure and state of stress. World Geothermal Congress, 19–25 April 2015, Melbourne, Australia. Conference proceedings.

Horváth, F., Musitz, B., Balázs, A., Végh, A., Uhrin, A., Nádor, A., Koroknai, B., Pap, N., Tóth, T. & Wórum, G., 2015. Evolution of the Pannonian basin and its geothermal resources. Geothermics **53**: 328–352.

Iglesias, E., Contreras L.E., Garcia G.A. & Dominquez A.B., 1987. Petrophysical properties of twenty drill cores from the Los Azufres, Mexico, Geothermal Field. 12th Workshop on Geothermal Reservoir Engineering, 20–22 January 1987, Stanford University, Stanford, California. Conference proceedings.

Ito, H., 2003. Inferred role of natural fractures, veins, and breccias in development of the artificial geothermal reservoir at the Ogachi Hot Dry Rock site, Japan. Journal of Geophysical Research: Solid Earth **108**(B9): 2426. doi: 10.1029/2001JB001671.

Juncu, D., Árnadóttir, T., Geirsson, H., Guðmundsson, G.B., Lund, B., Gunnarsson, G., Hooper, A., Hreinsdóttir, S. & Michalczewska, K., 2018. Injection-induced surface deformation and seismicity at the Hellisheidi geothermal field, Iceland. Journal of Volcanology and Geothermal Research.

Jung, R., 2013. EGS – goodbye or back to the future? ISRM International Conference for Effective and Sustainable Hydraulic Fracturing, 20–22 May 2013, Brisbane, Australia. Conference proceedings.

Jupe, A., Green, A. & Wallroth, T., 1992. Induced microseismicity and reservoir growth at the Fjällbacka hot dry rocks project, Sweden. International Journal of Rock Mechanics and Mining Sciences & Geomechanics Abstracts.

Kabus, F. & Jäntsch, E., 1995. The geothermal heating plant at Waren-Papenberg: experience and modernisation. World Geothermal Congress 18–31 May 1995, Florence, Italy. Conference proceedings: 2227–2232.

Kaieda, H., 2015. Multiple reservoir creation and evaluation in the Ogachi and Hijiori HDR projects, Japan. World Geothermal Congress, 19–25 April 2015, Melbourne, Australia. Conference proceedings.

Kaieda, H., Jones, R., Moriya, H., Sasaki, S. & Ushijima, K., 2005. Ogachi HDR reservoir evaluation by AE and geophysical methods. World Geothermal Congress, 24–29 April 2005, Antalya, Turkey. Conference proceedings.

Kang, J., Zhu, J. & Zhao, J., 2019. A review of mechanisms of induced earthquakes: from a view of rock mechanics. Geomechanics and Geophysics for Geo-Energy and Geo-Resources 5(2): 171–196.

Karytsas, C., Mendrinos, D. & Goldbrunner, J., 2009. Production monitoring at the Geinberg geothermal site. Energy Sources Part A 31(17): 1537–1552.

Kaya, E., Zarrouk, S.J. & O'Sullivan, M.J., 2011. Reinjection in geothermal fields: a review of worldwide experience. Renewable and Sustainable Energy Reviews 15(1): 47–68.

Kepinska, B., 2015. Geothermal energy country update report from Poland, 2010–2014. World Geothermal Congress, 19–25 April 2015, Melbourne, Australia. Conference proceedings.

Kim, K., Ree, J., Kim, Y., Kim, S., Kang, S.Y. & Seo, W., 2018a. Assessing whether the 2017 M_w 5.4 Pohang earthquake in South Korea was an induced event. Science (New York) 360(6392): 1007. doi:10.1126/science.aat6081.

Kim, K., Min, K., Kim, K., Choi, J.W., Yoon, K., Yoon, W.S., Yoon, B., Lee, T.J. & Song, Y., 2018b. Protocol for induced microseismicity in the first enhanced geothermal systems project in Pohang, Korea. Renewable and Sustainable Energy Reviews 91: 1182–1191.

Klose, C. D., 2007. Geomechanical modeling of the nucleation process of Australia's 1989 M5.6 Newcastle earthquake. Earth and Planetary Science Letters 256(3–4): 547–553.

Koh, J., Roshan, H. & Rahman, S.S., 2011. A numerical study on the long term thermo-poroelastic effects of cold water injection into naturally fractured geothermal reservoirs. Computers and Geotechnics 38(5): 669–682.

Kraft, T., Wiemer, S., Deichmann, N., Diehl, T., Edwards, B., Guilhem, A., … Woessner, J., 2013. The ML 3.5 earthquake sequence induced by the hydrothermal energy project in St. Gallen, Switzerland. American Geophysical Union, Fall Meeting 2013, Abstract S31F-03.

Kramers, L., Van Wees, J. D., Pluymaekers, M. P. D., Kronimus, A. & Boxem, T., 2012. Direct heat resource assessment and subsurface information systems for geothermal aquifers: the Dutch perspective. Netherlands Journal of Geosciences / Geologie en Mijnbouw 91(4): 637–649.

Kreemer, C., Blewitt, G. & Klein, E.C., 2014. A geodetic plate motion and global strain rate model. Geochemistry, Geophysics, Geosystems 15(10): 3849–3889.

Kristensen, L., Hjuler, M.L., Frykman, P., Olivarius, M., Weibel, R., Nielsen, L.H. & Mathiesen, A., 2016. Pre-drilling assessments of average porosity and permeability in the geothermal reservoirs of the Danish area. Geothermal Energy 4(1): 1–27. doi: 10.1186/s40517-016-0048-6.

Küperkoch, L., Olbert, K. & Meier, T., 2018. Long-term monitoring of induced seismicity at the Insheim geothermal site, Germany. Bulletin of the Seismological Society of America 108(6): 3668–3683.

Kurowska, E., 2000. Analysing reservoir properties of the Liassic sedimentary layer in Poland. Report No. 11. United Nations University (Reykjavik).

Kwiatek, G., Bohnhoff, M., Dresen, G., Schulze A., Schulte, T., Zimmermann, G. & Huenges, E., 2010. Microseismicity induced during fluid-injection: a case study from the geothermal site at Groß Schönebeck, North German Basin. Acta Geophysica 58(6): 995–1020.

Kwiatek, G., Bulut, F., Bohnhoff, M. & Dresen, G., 2014. High-resolution analysis of seismicity induced at Berlín geothermal field, El Salvador. Geothermics 52: 98–111.

Kwiatek, G., Saarno, T., Ader, T., Bluemle, F., Bohnhoff, M., Chendorain, M., Dresen, G., Heikkinen, P., Kukkonen, I. & Leary, P., 2019. Controlling fluid-induced seismicity during a 6.1-km-deep geothermal stimulation in Finland. Science Advances 5(5): eaav7224.

Lei, X., Wang, Z. & Su, J., 2019. The December 2018 ML 5.7 and January 2019 ML 5.3 earthquakes in South Sichuan basin induced by shale gas hydraulic fracturing. Seismological Research Letters 90: 1099–1110.

Lengline, O., Boubacar, M. & Schmittbuhl, J., 2017. Seismicity related to the hydraulic stimulation of GRT1, Rittershoffen, France. Geophysical Journal International 208(3): 1704–1715.

Lermo, J., Antayhua, Y., Quintanar, L. & Lorenzo, C., 2008. Estudio sismológico del campo geotérmico de Los Humeros, Puebla, México. Parte I: Sismicidad, mecanismos de fuente y distribución de esfuerzos. Geotermia: 25.

LIAG (Leibniz-Institut für Angewandte Geophysik), 2018. Untersuchung der Seismizität am Standort des Geothermieprojekts Poing unter Einbeziehung von Strukturgeologie, Geohydraulik, Hydrochemie, Geomechanik und Dublettenbetrieb. Zusammenfassung. LIAG (Hannover).

Lopez, S., Hamm, V., Le Brun, M., Schaper, L., Boissier, F., Cotiche, C. & Giuglaris, E., 2010. 40 years of Dogger aquifer management in Ile-de-France, Paris Basin, France. Geothermics 39: 339–356.

Lu, S., 2018. A global review of enhanced geothermal system (EGS). Renewable and Sustainable Energy Reviews 81: 2902–2921.

Lund, J.W., Bertani, R., & Boyd, T., 2015. Worldwide geothermal energy utilization 2015. GRC Transactions 39: 79–92.

Lutz, S.J., Hickman, S., Davatzes, N., Zemach, E., Drakos, P. & Robertson-Tait, A., 2010. Rock mechanical testing and petrologic analysis in support of well stimulation activities at the Desert Peak Geothermal Field, Nevada. Proceedings of the 35th Workshop on Geothermal Reservoir Engineering.

Mahler, A., 1995. Geothermal plant in Thisted with absorption heat pump and 10 years operation without corrosion or reinjection problems in sandstone for 15% saline water. World Geothermal Congress 18–31 May 1995, Florence, Italy. Conference proceedings.

Mahler, A., Røgen, B., Ditlefsen, C., Nielsen, L.H. & Vangkilde-Pedersen, T., 2013. Geothermal energy use, country update for Denmark. Proceedings of the European Geothermal Congress.

Majer, E. L., Freeman, K., Johnson, L., Jarpe, S., Nihei, K. T., Hartline, C., Walter, M. & Deniliger, M., 2017. Monitoring the effect of injection of fluids from the Lake County pipeline on seismicity at The Geysers, California, geothermal field. Final Report. Lawrence Berkeley National Laboratory, Calpine Corporation (Lake County, CA).

Martínez-Garzón, P., Kwiatek, G., Sone, H., Bohnhoff, M., Dresen, G. & Hartline, C., 2014. Spatiotemporal changes, faulting regimes, and source parameters of induced seismicity: a case study from The Geysers geothermal field. Journal of Geophysical Research: Solid Earth 119(11): 8378–8396.

Maurer, V., Cuenot, N., Gaucher, E., Grunberg, M., Vergne, J., Wodling, H., … Schmittbuhl, J., 2015. Seismic monitoring of the Rittershoffen EGS project (Alsace, France). World Geothermal Congress, 19–25 April 2015, Melbourne, Australia. Conference proceedings.

Mazzoldi, A., Borgia, A., Ripepe, M., Marchetti, E., Ulivieri, G., della Schiava, M. & Allocca, C., 2015. Faults strengthening and seismicity induced by geothermal exploitation on a spreading volcano, Mt. Amiata, Italia. Journal of Volcanology and Geothermal Research 301: 159–168.

McComas, K.A., Lu, H., Keranen, K.M., Furtney, M.A. & Song, H., 2016. Public perceptions and acceptance of induced earthquakes related to energy development. Energy Policy 99: 27–32.

McGarr, A., 2014. Maximum magnitude earthquakes induced by fluid injection. Journal of Geophysical Research: Solid Earth 119(2): 1008–1019.

McGuire, J.J., Lohman, R.B., Catchings, R.D., Rymer, M.J. & Goldman, M.R., 2015. Relationships among seismic velocity, metamorphism, and seismic and aseismic fault slip in the Salton Sea Geothermal Field region. Journal of Geophysical Research: Solid Earth 120(4): 2600–2615.

Megies, T. & Wassermann, J., 2014. Microseismicity observed at a non-pressure-stimulated geothermal power plant. Geothermics 52: 36–49.

Meixner, J., Schill, E., Grimmer, J.C., Gaucher, E., Kohl, T. & Klingler, P., 2016. Structural control of geothermal reservoirs in extensional tectonic settings: an example from the Upper Rhine Graben. Journal of Structural Geology 82: 1–15.

Meyer, Z. & Kozlowski, J., 1995. Pyrzyce-first geothermal heating system in Poland. World Geothermal Congress 18–31 May 1995, Florence, Italy. Conference proceedings.

Mignan, A., Landtwing, D., Kästli, P., Mena, B. & Wiemer, S., 2015. Induced seismicity risk analysis of the 2006 Basel, Switzerland, Enhanced Geothermal System project: influence of uncertainties on risk mitigation. Geothermics 53: 133–146.

Ministry of Economic Affairs and Climate Policy, 2018. Natural resources and geothermal energy in the Netherlands. Annual review 2017. Ministry of Economic Affairs and Climate Policy (The Hague).

Mitsumori, S., Asanuma, H., Adachi, M., Aoyama, K., Ozeki, H. & Saeki, K., 2012. Long term microseismic monitoring at Yanaizu-Nishiyama geothermal field, Japan. 18th Formation Evaluation Symposium of Japan: 7.

Moeck, I.S., 2014. Catalog of geothermal play types based on geologic controls. Renewable and Sustainable Energy Reviews 37: 867–882.

Moeck, I., Kwiatek, G. & Zimmermann, G., 2009. Slip tendency analysis, fault reactivation potential and induced seismicity in a deep geothermal reservoir. Journal of Structural Geology 31: 1174–1182.

Moeck, I., Bloch, T., Graf, R., Heuberger, S., Kuhn, P., Naef, H., . . . & Wolfgramm, M., 2015. The St. Gallen project: development of fault controlled geothermal systems in urban areas. World Geothermal Congress, 19–25 April 2015, Melbourne, Australia. Conference proceedings.

Moia, F., 2008. Individuazione ed applicazione di metodologie di monitoraggio di possibili fughe di CO2 dai serbatoi di stoccaggio. Report No. 08001015. Cesi Ricerca (Milan).

Monterrosa, M. & López, F.E.M., 2010. Sustainability analysis of the Ahuachapán geothermal field: management and modeling. Geothermics 39(4): 370–381.

Mossop, A. & Segall, P., 1997. Subsidence at The Geysers Geothermal Field, N. California from a comparison of GPS and leveling surveys. Geophysical Research Letters 24(14): 1839–1842.

Moya, P. & Nietzen, F., 2010. Production-injection at the Miravalles Geothermal Field, Costa Rica. World Geothermal Congress, 25–29 April 2010, Bali, Indonesia. Conference proceedings.

Moya, P. & Taylor, W., 2010. Micro-seismicity at the Miravalles Geothermal Field, Costa Rica (1994–2009): a tool to confirm the real extent of the reservoir. World Geothermal Congress, 25–29 April 2010, Bali, Indonesia. Conference proceedings.

Obermann, A., Kraft, T., Larose, E. & Wiemer, S., 2015. Potential of ambient seismic noise techniques to monitor the St. Gallen geothermal site (Switzerland). Journal of Geophysical Research: Solid Earth 120(6): 4301–4316.

Orzol, J., Jung, R., Jatho, R., Tischner, T. & Kehrer, P., 2005. The GeneSys-Project: extraction of geothermal heat from tight sediments. World Geothermal Congress, 24–29 April 2005, Antalya, Turkey. Conference proceedings.

Panzera, F., Mignan, A. & Vogfjörð, K.S., 2017. Spatiotemporal evolution of the completeness magnitude of the Icelandic earthquake catalogue from 1991 to 2013. Journal of Seismology 21(4): 615–630.

Parker, R., 1999. The Rosemanowes HDR project 1983–1991. Geothermics 28: 603–615.

Pawley, S., Schultz, R., Playter, T., Corlett, H., Shipman, T., Lyster, S. & Hauck, T., 2018. The geological susceptibility of induced earthquakes in the Duvernay play. Geophysical Research Letters 45(4): 1786–1793.

Phillips, W.S., House, L.S. & Fehler, M.C., 1997. Detailed joint structure in a geothermal reservoir from studies of induced microearthquake clusters. Journal of Geophysical Research: Solid Earth 102(B6): 11745–11763.

Pilger, M., Eulenfeld, T., Brüstle, A., Wegler, U., Plenefisch, T. & Schmidt, B., 2017. Mikroseismische Aktivität geothermischer Systeme 2 – Vom Einzelsystem zur grossräumigen Nutzung. Einzelprojekt 1 – Seismische Monitoringskonzepte und bruchmechanische Bewertungen für komplexe Geothermiefelder am Beispiel Südpfalz. Report No. 0325662A. Bundesanstalt für Geowissenschaften und Rohstoffe (Hannover).

Prol-Ledesma, R.M., Arango-Galvan, C. & Torres-Vera, M., 2016. Rigorous analysis of available data from Cerro Prieto and Las Tres Vírgenes geothermal fields with calculations for expanded electricity generation. Natural Resources Research 25(4): 445–458.

Prol-Ledesma, R.M. & Morán-Zenteno, D.J., 2019. Heat flow and geothermal provinces in Mexico. Geothermics 78: 183–200.

Ragnarsson, Á., 2005. Geothermal development in Iceland 2000–2004. World Geothermal Congress, 24–29 April 2005, Antalya, Turkey. Conference Proceedings.

Reinecker, J., Tingay, M., Müller, B. & Heidbach, O., 2010. Present-day stress orientation in the Molasse Basin. Tectonophysics 482(1): 129–138.

Reith, D.F.H., 2018. Dynamic simulation of a geothermal reservoir: case study of the dinantian carbonates in the Californië geothermal wells. MSc Thesis. TU Delft (Limburg).

Richards, H.G., Parker, R.H., Green, A.S.P., Jones, R.H., Nicholls, J.D.N., Nicol, D.A.C., Randall, M.M., Richards, S., Stewart, R.C. & Willis-Richards, J., 1994. The performance and characteristics of the experimental hot dry rock geothermal reservoir at Rosemanowes, Cornwall. Geothermics 23(2): 73–109.

Riffault, J., Dempsey, D., Archer, R., Kelkar, S. & Karra, S., 2016. Understanding poroelastic stressing and induced seismicity with a stochastic/deterministic model: an application to an EGS stimulation at Paralana, South Australia, 2011. 41st Workshop on Geothermal Reservoir Engineering, 22–24 February 2016, Stanford, California. Conference proceedings. SGPTR-209.

Rioseco, E.M., Löhken, J., Schellschmidt, R. & Tischner, T., 2013. 3-D geomechanical modeling of the stress field in the North German basin: case study GeneSys-borehole GT1 in Hanover Groß-Buchholz. 38th Workshop on Geothermal Reservoir Engineering, 11–13 February 2013, Stanford, California. Conference proceedings.

Rivas, J.A., Castellón, J.A. & Maravilla, J.N., 2005. Seven years of reservoir seismic monitoring at Berlın Geothermal Field, Usulután, El Salvador. World Geothermal Congress, 24–29 April 2005, Antalya, Turkey. Conference proceedings.

Rodríguez, S. & Aníbal, V., 2005. Analysis of temperature and pressure measurements and production data for Berlin geothermal field, El Salvador. UNU Geothermal Training Programme, Iceland. Report 2005-16. United Nations University (Orkustofnun).

Røgen, B., Ditlefsen, C., Vangkilde-Pedersen, T., Nielsen, L. H. & Mahler, A., 2015. Geothermal energy use, 2015 country update for Denmark. World Geothermal Congress, 19–25 April 2015, Melbourne, Australia. Conference proceedings.

Rojas, J., Giot, D., Le Nindre, Y. M., Criaud, A., Fouillac, C., Brach, M., . . . & Pauwels, H., 1989. Caractérisation et modélisation du réservoir géothermique du Dogger Bassin Parisien, France. Report No. BRGM/RR-30169-FR. BRGM (Orléans).

Rutqvist, J., Dobson, P.F., Garcia, J., Hartline, C., Jeanne, P., Oldenburg, C.M., Vasco, D.W. & Walters, M., 2015. The northwest Geysers EGS demonstration project, California: pre-stimulation modeling and interpretation of the stimulation. Mathematical Geosciences 47(1): 3–29.

Sasaki, S. & Kaieda, H., 2002. Determination of stress state from focal mechanisms of microseismic events induced during hydraulic injection at the Hijiori hot dry rock site. Pure and Applied Geophysics 159: 489–516.

Scheck-Wenderoth, M. & Lamarche, J., 2005. Crustal memory and basin evolution in the Central European Basin System: new insights from a 3D structural model. Tectonophysics 397(1): 143–165.

Schindler, M., Baumgärtner, J., Gandy, T., Hauffe, P., Hettkamp, T., Menzel, H., . . . & Wahl, G., 2010. Successful hydraulic stimulation techniques for electric power production in the Upper Rhine Graben, Central Europe. World Geothermal Congress, 25–29 April 2010, Bali, Indonesia. Conference proceedings.

Schoenball, M., Baujard, C., Kohl, T. & Dorbath, L., 2012. The role of triggering by static stress transfer during geothermal reservoir stimulation. Journal of Geophysical Research: Solid Earth 117(B9), B09307. doi: 10.1029/2012jb009304.

Segall, P., 1989. Earthquakes triggered by fluid extraction. Geology 17(10): 942–946.

Segall, P. & Fitzgerald, S. D., 1998. A note on induced stress changes in hydrocarbon and geothermal reservoirs. Tectonophysics 289: 117–128.

Seibt, P., Kabus, F. & Hoth, P., 2005. The Neustadt-Glewe geothermal power plant: practical experience in the reinjection of cooled thermal waters into

sandstone aquifers. World Geothermal Congress, 24–29 April 2005, Antalya, Turkey. Conference proceedings.

Seithel, R., Gaucher, E., Mueller, B., Steiner, U. & Kohl, T., 2019. Probability of fault reactivation in the Bavarian Molasse Basin. Geothermics **82**: 81–90.

Sewell, S., Cumming, W., Bardsley, C., Winick, J., Quinao, J., Wallis, I., Sherburn, S. & Bourguignon, S., 2015. Interpretation of microseismicity at the Rotokawa geothermal field, 2008 to 2012. World Geothermal Congress, 19–25 April 2015, Melbourne, Australia. Conference proceedings.

Shapiro, S. A. & Dinske, C., 2009. Fluid-induced seismicity: pressure diffusion and hydraulic fracturing. Geophysical Prospecting **57**: 301–310.

Sherburn, S., Bromley, C., Bannister, S., Sewell, S. & Bourguignon, S., 2015a. New Zealand geothermal induced seismicity: an overview. World Geothermal Congress, 19–25 April 2015, Melbourne, Australia. Conference proceedings.

Sherburn, S., Sewell, S., Bourguignon, S., Cumming, W., Bannister, S., Bardsley, C., Winick, J., Quinao, J. & Wallis, I., 2015b. Microseismicity at Rotokawa geothermal field, New Zealand, 2008–2012. Geothermics **54**: 23–34.

Soltanzadeh, H. & Hawkes, C.D., 2008. Semi-analytical models for stress change and fault reactivation induced by reservoir production and injection. Journal of Petroleum Science and Engineering **60**(2): 71–85.

Soltanzadeh, H. & Hawkes, C.D., 2009. Induced poroelastic and thermoelastic stress changes within reservoirs during fluid injection and production. Porous Media: Heat and Mass Transfer, Transport and Mechanics **2009**: 27–57.

Sone, H. & Zoback, M.D., 2014. Time-dependent deformation of shale gas reservoir rocks and its long-term effect on the in situ state of stress. International Journal of Rock Mechanics and Mining Sciences **69**: 120–132.

Sowizdzal, A., 2018. Geothermal energy resources in Poland: overview of the current state of knowledge. Renewable and Sustainable Energy Reviews **82**: 4020–4027.

Spetzler, J., Ruigrok, E., Dost, B. & Evers, L., 2018. Hypocenter estimation of detected event near Venlo on September 3rd 2018. Technical Report. Report No. 369. KNMI (De Bilt).

State Supervision of Mines, 2019. Analyse onderbouwing CLG aardwarmte en seismiciteit. Technical Report. State Supervision of Mines (The Hague).

State Supervision of Mines & TNO-AGE, 2013. Protocol bepaling maximale injectiedrukken bij aardwarmtewinning – versie 2. State Supervision of Mines (The Hague); TNO-AGE, https://www.sodm.nl/documenten/publicaties/2013/11/23/protocol-bepaling-maximale-injectiedrukken-bij-aardwarmtewinning

Stefansson, V., 1997. Geothermal reinjection experience. Geothermics **26**(1): 99–139.

Stichting Platform Geothermie, DAGO, Stichting Warmtenetwerk & EBN., 2018. Masterplan Aardwarmte in Nederland. www.ebn.nl/publicatie/het-masterplan-aardwarmte-nederland/

Szanyi, J. & Kovács, B., 2010. Utilization of geothermal systems in South-East Hungary. Geothermics **39**(4): 357–364.

Szita, G. & Vitai, Z., 2013. Successful injection of geothermal water into sandstones: an example from Hungary. Technika Poszukiwań Geologicznych **52**(2): 201–206.

Tischner, T., Krug, S., Pechan, E., Hesshaus, A., Jatho, R., Bischoff, M. & Wonik, T., 2013. Massive hydraulic fracturing in low permeable sedimentary rock in the GeneSys project. 38th Workshop on Geothermal Reservoir Engineering, 11–13 February 2013, Stanford, California. Conference proceedings.

Tosha, T., Nishikawa, N., Shimada, T. & Oishi, T., 2016. Country update of geothermal energy development in Japan and the activity of JOGMEC. GRC Transactions 40. Geothermal Resources Council (Davis, CA).

Tóth, L., Mónus, P., Bus, Z. & Győri, E., 2008. Seismicity of the Pannonian Basin. In: E.S. Husebye & C. Christova (eds): Earthquake monitoring and seismic hazard mitigation in Balkan countries. Springer (New York): 99–110.

Trugman, D.T., Borsa, A.A. & Sandwell, D.T., 2014. Did stresses from the Cerro Prieto Geothermal Field influence the El Mayor-Cucapah rupture sequence? Geophysical Research Letters **41**(24): 8767–8774.

Trugman, D.T., Shearer, P.M., Borsa, A.A. & Fialko, Y., 2016. A comparison of long-term changes in seismicity at The Geysers, Salton Sea, and Coso geothermal fields. Journal of Geophysical Research: Solid Earth **121**(1): 225–247.

Ungemach, P., Antics, M. & Papachristou, M., 2005. Sustainable geothermal reservoir management. World Geothermal Congress, 24–29 April 2005, Antalya, Turkey. Conference proceedings.

Urban, E. & Lermo, J.F., 2012. Relationship of local seismic activity, injection wells and active faults in the geothermal fields of Mexico. Proceedings of Thirty-Seventh Workshop on Geothermal Reservoir Engineering, Stanford University, Stanford, CA, SGP-TR-194

Urban, E. & Lermo, J.F., 2013. Local seismicity in the exploitation of Los Humeros geothermal Field, Mexico. 38th Workshop on Geothermal Reservoir Engineering, 11–13 February 2013, Stanford, CA. Conference proceedings.

Van Wees, J.D., Kronimus, A., Van Putten, M., Pluymaekers, M., Mijnlieff, H., Van Hooff, P., Obdam, A. & Kramers, L., 2012. Geothermal aquifer performance assessment for direct heat production: methodology and application to Rotliegend aquifers. Netherlands Journal of Geosciences / Geologie en Mijnbouw **91**(4): 651–665.

Veldkamp, J.G., Mijnlieff, H., Bloemsma, M., Donselaar, R., Henares, S., Redjosentono, A. & Weltje, G.J., 2015. Permian Rotliegend reservoir architecture of the Dutch Koekoekspolder Geothermal Doublet. World Geothermal Congress, 19–25 April 2015, Melbourne, Australia. Conference proceedings.

Verma, S.P., Pandarinath, K., Santoyo, E., González-Partida, E., Torres-Alvarado, I. S. & Tello-Hinojosa, E., 2006. Fluid chemistry and temperatures prior to exploitation at the Las Tres Vírgenes geothermal field, Mexico. Geothermics **35**(2): 156–180.

Vidal, J. & Genter, A., 2018. Overview of naturally permeable fractured reservoirs in the central and southern Upper Rhine Graben: insights from geothermal wells. Geothermics **74**: 57–73.

Vondrak, A., Van de Weerd, A., Van Leeuwen, L. & Brautigam, K., 2014. Update doubletvoorstel HON-GT-03 en HON-GT-04. Report No. G1121. Panterra Consultants B.V. (Leiderdorp).

Vörös, R. & Baisch, S., 2019. Seismic hazard assessment for the CLG-Geothermal System – study update March 2019. Report No. CLG006. Q-con GmbH (Bad Bergzabern).

Wanner, C., Eichinger, F., Jahrfeld, T. & Diamond, L. W., 2017. Causes of abundant calcite scaling in geothermal wells in the Bavarian Molasse Basin, Southern Germany. Geothermics **70**: 324–338.

Wiemer, S., Kraft, T., Trutnevyte, E. & Roth, P., 2017. 'Good practice' guide for managing induced seismicity in deep geothermal energy projects in Switzerland. Report. Swiss Seismological Service (Zürich). doi: 10.3929/ethz-b-000254161

Willems, C.J.L., 2012. Study of the Lower Cretaceous sands in the Van den Bosch geothermal energy concession. MSc Thesis. TU Delft (Delft).

Willems, C.J., Nick, H.M., Weltje, G.J. & Bruhn, D.F., 2017. An evaluation of interferences in heat production from low enthalpy geothermal doublets systems. Energy **135**: 500–512.

Wilson, C.J. & Rowland, J.V., 2016. The volcanic, magmatic and tectonic setting of the Taupo Volcanic Zone, New Zealand, reviewed from a geothermal perspective. Geothermics **59**: 168–187.

Yeck, W.L., Weingarten, M., Benz, H.M., McNamara, D.E., Bergman, E.A., Herrmann, R.B., ... & Earle, P.S., 2016. Far-field pressurization likely caused one of the largest injection induced earthquakes by reactivating a large preexisting basement fault structure. Geophysical Research Letters, **43**(19), 198–207.

Zang, A., Oye, V., Jousset, P., Deichmann, N., Gritto, R., McGarr, A., Majer, E. & Bruhn, D., 2014. Analysis of induced seismicity in geothermal reservoirs: an overview. Geothermics **52**: 6–21.

Zhang, Y., Person, M., Rupp, J., Ellett, K., Celia, M.A., Gable, C.W., Bowen, B., Evans, J., Bandilla, K., & Elliot, T., 2013. Hydrogeologic controls on induced seismicity in crystalline basement rocks due to fluid injection into basal reservoirs. Groundwater **51**: 525–538.

Zimmermann, G., Moeck, I. & Blöcher, G., 2010. Cyclic waterfrac stimulation to develop an enhanced geothermal system (EGS): conceptual design and experimental results. Geothermics **39**(1): 59–69.

Zoback, M.D. & Townend, J., 2001. Implications of hydrostatic pore pressures and high crustal strength for the deformation of intraplate lithosphere. Tectonophysics **336**: 19–30.